Clarence Michael Cornforth

HIGH MAGNETIC FIELD PROPERTIES OF

GADOLINIUM, TERBIUM, AND HOLMIUM,

HIGH MAGNETIC FIELD PROPERTIES OF GADOLINIUM, TERBIUM, AND HOLMIUM

by

Clarence Michael Cornforth

An Abstract of

A Dissertation Submitted to the

Graduate Faculty in Partial Fulfillment of

The Requirements for the Degree of

DOCTOR OF PHILOSOPHY

Approved:

HIGH MAGNETIC FIELD PROPERTIES OF GADOLINIUM, TERBIUM, AND HOLMIUM*

Clarence Michael Cornforth

Under the supervision of Sam Legvold
From the Department of Physics
Iowa State University of Science and Technology

A vibrating sample magnetometer was used to measure magnetizations of Gd, Tb, and Tm in fields up to 100 kOe. Gd was found to have a spontaneous saturation magnetization at 4.2 K of 7.49 μ_B per atom and a high field susceptibility of 3.3×10^{-5} emu/gOe. The density of states at the Fermi energy was calculated to be 3.3×10^{34}/erg-cm^3 and the interaction energy between ions and conduction electrons found to be 1.26×10^{-13} erg. Tb had a spontaneous saturation magnetization at 4.2 K of 9.28 μ_B per atom and a high field susceptibility of 7.3×10^{-5} emu/gOe. Calculations of the density of states at the Fermi energy and the interaction energy between ions and conduction electrons gave 5.74×10^{34}/erg-cm^3 and 4.3×10^{-14} erg respectively. A transition from anti-ferromagnetic structure to anti-phase structure was found for holmium at 12 K.

*USAEC Report IS-T-277. This work was performed under contract W-7405-wng-82 with the Atomic Energy Commission.

HIGH MAGNETIC FIELD PROPERTIES OF GADOLINIUM, TERBIUM, AND HOLMIUM

by

Clarence Michael Cornforth

A Dissertation Submitted to the

Graduate Faculty in Partial Fulfillment of

The Requirements for the Degree of

DOCTOR OF PHILOSOPHY

Major Subject: Physics

TABLE OF CONTENTS

I. INTRODUCTION

Gadolinium, terbium and holmium belong to the transition group of elements beginning with lanthanum, atomic number 57, and ending with lutetium, atomic number 71. Commonly known as rare earths, they are distinguished from the remainder of the periodic table of elements by their nearly identical chemical properties and by certain unusual magnetic and electrical characteristics. This unusual behavior may be explained by noting the electronic configuration of the rare earths: $(4f)^n$ $(5s)^2$ $(5p)^6$ $(5d)^1$ $(6s)^2$. Here n ranges from zero to fourteen across the series. Since the $(5d)^1$ and $(6s)^2$ electrons are the valence electrons , the rare earths will have very similar chemical characteristics. Exceptions to this are cerium and terbium which may have four valence electrons and europium and ytterbium which may have two valence electrons . Apart from these, the rare earths are trivalent and form hexagonal close-packed crystal structures.

The magnetic properties and to some extent the electrical properties of the rare earth metals are to a large extent due to the 4f electrons and the manner in which these interact. Since the 4f electrons are tightly bound, magnetic ordering must take place through indirect exchange via the conduction electrons (1). Previous measurements of magnetic properties of rare earth metals (2), (3), (4), (5), (6), (7) have shown that the magnetic susceptibilities are very anisotropic, hence we must use single crystals for experimental studies of the metals.

Gadolinium, atomic number 64, has seven 4f electrons which half fill the shell. Neutron diffraction studies by Will et al. (8) report that gadolinium is a classical ferromagnetic substance below the Curie temperature

which is stated to be about 300 K. Later neutron diffraction studies by Koehler (9) confirm the classical ferromagnetic structure. Most recent neutron diffraction studies by Cable and Wollan (10) report a Curie temperature of 294 K with the c-axis the easy direction from 294 K to 232 K and a cone of magnetization with maximum deviation of 65^{o} from the c-axis and approaching 32^{o} at low temperature.

Magnetization measurements by Nigh (2) indicate a Curie temperature of 293.2 K, classical ferromagnetic behavior, and a saturation magnetization of 7.55 Bohr magnetons per atom in the c-axis direction. Less comprehensive magnetization measurements by Graham (11) give a Curie temperature of 292.5 ± 0.5 K.

Corner, et al. (12) using a torque magnetometer report that above 240 K, the easy direction is the c-axis and below 240 K it lies in a cone whose axis is the c-axis.

Nigh (2) has performed magnetization measurements up to 20 kilo-Oersteds and Rhyne et al. (13) have done magnetization experiments in fields up to 150 kilo-Oersteds to determine anisotropy energies. Féron and Pauthenet (14) have carried out magnetization measurements in fields up to 80 kilo-Oersteds and report a spontaneous saturation magnetization of 7.39 Bohr magnetons per atom with a superposed high field susceptibility of 45×10^{-6} electro-magnetic units per gram-Oersted in the c-axis direction.

Other properties of gadolinium which have been measured are: electrical resistivity by Nigh (2), Nellis (15); thermal conductivity by Nellis (15); Seebeck coefficient by Sill (16); Hall effect by Lee (17).

Terbium, atomic number 65, has the electronic structure: $(4f)^{8}$ $(5s)^{2}$ $(5p)^{6}$ $(5d)^{1}$ $(6s)^{2}$. Neutron diffraction studies by Koehler et al.

(18) report terbium has a Néel temperature at about 230 K. Below this temperature terbium has a helical anti-ferromagnetic structure with a turn angle along the c-axis varying from 20.5° per layer at the Néel temperature to 18.5° per layer at about 220 K, the Curie temperature, at which temperature it goes into a classical ferromagnetic structure with the moment perpendicular to the c-axis. Later neutron diffraction studies by Dietrich and Als-Nielsen (19) report a Néel temperature of 226 K, a Curie temperature of 216 K with turn angles per layer of 20.7° and 16.5° at 226 K and 216 K respectively.

Hegland (3) has done magnetization measurements in fields up to 20 kilo-Oersteds and reports a Néel temperature of 229° K, a Curie temperature of 221° K with a saturation magnetization of 9.34 Bohr magnetons in the b-axis direction. Magnetization measurements have been performed by Rhyne et al. (13) in fields up to 150 kilo-Oersteds giving saturation magnetization values in excess of 320 emu/g in the b-axis direction. The latest magnetization measurements in fields up to 80 kilo-Oersteds done by Féron and Pauthenet (14) gave a spontaneous saturation magnetization of 9.28 Bohr magnetons with a superposed high field magnetic susceptiblity of 52×10^{-6} emu/gOe.

Other properties of terbium which have been measured are: electrical resistivity by Hegland (3), Nellis (15);thermal conductivity by Nellis (15); Seebeck coefficient by Sill (16).

Holmium, atomic number 66, is structured electronically as: $(4f)^{10}$ $(5s)^{2}$ $(5p)^{6}$ $(5d)^{1}$ $(6s)^{2}$. Neutron diffraction studies by Koehler et al. (20) show that holmium has a Néel temperature of 133 K with a helical spin structure about the c-axis of the hexagonal crystal; the turn angles vary

from 50^{o} per layer at the Néel temperature to 30^{o} per layer at 4.2 K. Later neutron diffraction results reported by Koehler et al. (21) confirm the earlier diffraction studies and report that the b-axis is the easy direction of magnetization at low temperatures.

Magnetization measurements up to 20 kilo-Oersteds by Strandburg (5) indicate a Néel temperature of 132 K, a Curie temperature of 20 K with a saturation magnetization of 10.34 Bohr magnetons in the b-axis direction. Rhyne et al. (13) have done magnetization measurements in fields up to 150 kilo-Oersteds and report a saturation magnetization of 340 emu/g in the b-axis direction. Recent magnetization measurements in fields up to 80 kilo-Oersteds by Féron and Pauthenet (14) gave a spontaneous saturation magnetization of 10.22 Bohr magnetons per atom and a superposed high magnetic field susceptibility of 63×10^{-6} emu/gOe in the b-axis direction.

Other properties of holmium which have been measured are: electrical resistivity by Strandburg (5), Nellis (15);thermal conductivity by Nellis (15);Seebeck coefficient by Sill (16).

The purpose of this dissertation is to report experimental determinations of the high magnetic field susceptibilities of gadolinium and terbium; and to report the behavior of the critical magnetic field versus temperature for holmium. An additional goal is to elaborate on certain methods of measuring magnetization in superconductive solenoids.

II. BASIC CONCEPTS AND EQUATIONS

The magnetic susceptibility per gram is defined:

$$\sigma_g = \chi_g H , \qquad (2.1)$$

where χ_g is the susceptibility per gram, σ_g is the magnetization per gram, and H is the magnetic field intensity.

Solids show three general types of magnetic behavior. Diamagnetic substances have small, negative, and largely temperature independent susceptibilities. Paramagnetic materials have small to moderate and positive susceptibilities which do vary with temperature. Ferromagnetic solids are distinguished from other magnetic materials by having large magnetizations even when no magnetic field is applied (spontaneous magnetization). Susceptibilities for ferromagnetic substances are large, positive, and are strongly dependent on both temperature and applied magnetic field.

The common approach to the rare earth metals is to visualize them as a lattice of positive ions surrounded by a sea of free electrons. The free electrons are the three valence electrons and make up conduction bands which are combinations of s and d wave function character. The ions have an unfilled 4f shell which is screened by 5s and 5p electrons and are therefore tightly bound to the ion.

The heavy rare earth metals (Gd through Tm) are hexagonal close packed with c/a ratios varying from 1.57 to 1.59. Since the unfilled 4f shell provides the receptacle for electrons in the series, the Fermi surfaces and the band structures vary only slightly from element to element. Hence, the magnetic properties of these heavy rare earth metals must be explained by the behavior of the unfilled 4f shell.

The magnetic properties of the rare earth metals may be explained by means of two exchange interactions. The first is a direct exchange between ions; the second is an indirect exchange between ions via the conduction electrons.

By first ignoring the exchange interactions, we can calculate a paramagnetic susceptibility. According to quantum theory, the magnetic moment of an ion is not free, but is constrained to a limited set of orientations relative to the applied magnetic field. If an ion has total angular momentum J, the 2J+1 components of the magnetic moment are:

$$m_j \; g \; \mu_B \tag{2.2}$$

where mj = J, (J+L), ..., (-J+1), -J, g is the Landé splitting factor obtained by projecting the magnetic moment $\underline{L} + 2\underline{s}$ upon $\underline{J}$ in the lowest Russell-Saunders multiplet,

$$g = (\underline{L} + 2\underline{s}) \cdot \underline{J}/J^2 \; , \tag{2.3}$$

and μ_B is the Bohr magneton.

Using statistical mechanics the magnetization is given by:

$$\sigma_g = Ng \; J \; \mu_B \; B_J \; (\chi). \tag{2.4}$$

where N is the number of ions per gram, $B_J(\chi)$ is the Brillouin function (see Dekker (22) p. 455); and

$$x = g \; J \; \mu_B \; H/kT. \tag{2.5}$$

where K is the Boltzmann constant and T is the temperature.

In the case of high temperatures or low magnetic energy, $g \; J \; \mu_B \; H$ is much less than the thermal energy kT (i.e. $x \ll 1$), and the equation (2.4) reduces to:

$$\sigma_g = \frac{NJ(J+1)\, g^2\, \mu_B^2\, H}{3kT} \quad . \tag{2.6}$$

Then using equation (2.1)

$$\chi_g = \frac{NJ(J+1)\, g^2\, \mu_B^2}{3kT} = \frac{Cg}{T} , \tag{2.7}$$

where

$$Cg = \frac{NJ(J+1)\, g^2\, \mu_B^2}{3kT} \quad . \tag{2.8}$$

When the exchange interaction is included a more accurate description of magnetic behavior for the rare earth metals emerges.

The most important exchange interaction is the ion-ion exchange interaction. Heisenberg (23) postulated an exchange Hamiltonian of the form:

$$\mathcal{H} = -2 \sum_{i,j} V(\underline{R}i - \underline{R}j)\, \underline{S}i \cdot \underline{S}j \quad . \tag{2.9}$$

where $\underline{R}i$ is the position of the i^{th} ion possessing spin $\underline{S}i$, $\underline{R}i$ is the position of the j^{th} ion with spin $\underline{S}j$, and $V(\underline{R}i - \underline{R}j)$ is the exchange term. Since the exchange energy is considerably smaller than the splitting of the J multiplets by the spin-orbit ($\underline{L}$, $\underline{S}$) coupling, we should use the projection of $\underline{S}$ upon the total momentum $\underline{J}$, or

$$\underline{S} = (g - 1)\, \underline{J} \quad . \tag{2.10}$$

Introducing an applied field $\underline{H}a$, then

$$\mathcal{H} = -2 \sum_{i,j} V(\underline{R}i - \underline{R}j)(g - 1)^2\, \underline{J}i \cdot \underline{J}j - \sum_i \mu_B\, g\, \underline{J}i \cdot \underline{H}a \, . \tag{2.11}$$

In the heavy rare earth metals, the ordering is in planar layers perpendicular to the hexagonal axis. Hence, summing in layers and considering the interactions between nearest and next nearest neighbors

along the c-axis (see Elliott (24)) gives:

$$\mathcal{H} = -N[2(g-1)^2 V(0) \underline{J} + \mu_B g \underline{Ha}] \cdot \underline{J} , \tag{2.12}$$

with $V(0) = V_o + ZV_1 + ZV_2$ in which V_o is the exchange between 4f electrons in the same layer, V_1 is the exchange between nearest layers, and V_2 is the exchange between next nearest layers.

Then using $\langle \mathcal{H} \rangle = E$ and $\langle Ng \mu_B \underline{J} \rangle = \underline{\sigma}_g$

$$E = - \left[\frac{2(g-1)^2 V(0)}{g^2 \mu_B^2 N} \underline{\sigma}_g + \underline{Ha} \right] \cdot \underline{\sigma}_g . \tag{2.13}$$

Identifying the term in brackets as the Weiss molecular field (see Ziman (25) p. 289) gives

$$\lambda = \frac{2(g-1)^2 V(0)}{g^2 \mu_B^2 N} . \tag{2.14}$$

Replacing H in equation (2.5) by $Ha + \lambda \sigma_g$ gives

$$\sigma_g = Ng J \mu_B B_J \left[\frac{gJ\mu_B}{kT} (Ha + \lambda \sigma_g) \right], \tag{2.15}$$

the new counterpart of equation (2.4). Once again if $g J \mu_B Ha \ll kT$ then

$$X_g = C_g/T - \theta_c , \tag{2.16}$$

where

$$\theta_c = \lambda C_g . \tag{2.17}$$

In the limit $T \to 0$, $Ha \to \infty$

$$\sigma_g (0, \infty) = Ng J \mu_B . \tag{2.18}$$

Hence the effective number of Bohr magnetons at saturation is given by

$$N_{eff} = g J . \tag{2.19}$$

In addition to the exchange between ions, there is also an indirect exchange carried between ions by the conduction electrons. The indirect exchange was first used for nuclear coupling by Ruderman and Kittel (26). The indirect exchange concept was first applied to rare earth metals by de Gennes (27) and Liu (28). Liu assumed a Hamiltonian made up of the Kinetic energy of the electrons; the interactions between the ions and the applied magnetic field; between electrons and ions; and between electrons and the field. Thence

$$\mathcal{H} = \sum_i (Pi^2/2m) + \sum_{i,j} I\, \Omega_o\, \underline{s}i \cdot \underline{S}j\, \delta(\underline{r}i - \underline{R}i) \qquad (2.20)$$

$$- \sum_j g\, \mu_B\, \underline{Ha} \cdot \underline{S}j - \sum_i 2\, \mu_B\, \underline{Ha} \cdot \underline{s}i \quad .$$

where Ω_o is the volume of the ion, I the energy of electron-ion coupling S's are ion spins, s's are electron spins, and the ion-electron interaction is localized by the delta function.

Assuming a free electron model,

$$\Psi(\underline{r}) = \Omega^{-1/2}\, U_\sigma \exp(i\, \underline{K} \cdot \underline{r}) \,. \qquad (2.21)$$

where Ω is the volume over which the wave function is normalized U_σ is a Pauli spinor. From this point it can be shown (29), (30) that

$$E = E_o - \frac{1}{2}\, \chi_p \left(\frac{I}{2\mu_B N}\right)^2 \left(\sum_j \bar{S}_j^z\right)^2$$

$$-\left(g\, \mu_B - \frac{I\, \chi_p}{2\mu_B N}\right) Ha \sum_j \bar{S}_j^z - \frac{1}{2}\, \chi_p\, Ha^2 . \qquad (2.22)$$

where

$$\chi_p = 2\, \mu_B^2\, N(E_F) \quad , \qquad (2.23)$$

the Pauli spin paramagnetism with $N(E_F)$ the density of electron states at the Fermi surface.

Now because of the polarization of the conduction electrons, we may replace g as given by equation (2.3) by g' where

$$g' = g - \frac{I \chi_p}{2\mu_B^2 N} \quad . \tag{2.24}$$

Note that since $\chi_p \left(\frac{I}{2\mu_B N}\right)^2$ is greater than zero, the term $-1/2\ \chi_p \left(\frac{I}{2\mu_B N}\right)^2 \left(\sum_j S_j^z\right)^2$ requires a state of ordered spin (i.e. $\sum_j S_i^z \neq 0$) to minimize the energy, and explains that the ferromagnetic state is more stable at low temperatures than other less ordered states.

At $T = 0^oK$, all the spins will be aligned, hence the spontaneous magnetization should be

$$\sigma_o = g' \mu_B SN \ , \tag{2.25}$$

and

$$\sigma_o = \sigma_i + \sigma_e \quad . \tag{2.26}$$

Where σ_i is the ionic magnetization written

$$\sigma_i = g \mu_B SN \ . \tag{2.27}$$

σ_e is the electronic saturation written

$$\sigma_e = - I \chi_p S/2 \mu_B \ , \tag{2.28}$$

and from equation (2.23)

$$\sigma_e = - IS \mu_B N(E_F) \ . \tag{2.29}$$

Now, if the term $\chi_p \left(\frac{I}{2\mu_B N}\right)^2 \left(\sum_i S_i^z\right)^2$ in equation (2.22) is identified

with the term $\frac{z(g-1)\ V(0)\ \sigma_g^{\ 2}}{g^2 \mu_B^{\ 2}\ N}$ in equation (2.13) then

$$\frac{1}{2}\ \chi_p\ \left(\frac{1}{2\mu_B N}\right)^2 = \lambda (g')^2\ \mu_B^{\ 2}\ . \tag{2.30}$$

From equations (2.17) and (2.8)

$$\theta_c = \frac{I^2\ J(J+1)\ N(E_F)}{12kN}\ \left(\frac{g}{g'}\right)^2 \tag{2.31}$$

The critical field can be related to the magnetic moment by using the following expression for H_c:

$$(\langle\ |\ \mu\ |\ \rangle_\lambda - \langle\ \mu\ \rangle_\lambda)\ H_c = F_F - F_P\ . \tag{2.32}$$

$\langle\ \mu\ \rangle_\lambda$ is the value of the magnetic moment averaged over the wavelength of the helical or periodic spin structure. $|\ \mu\ |$ is the absolute value of μ. F_F is the free energy of the ferromagnetic state and F_p is the free energy of the helical or periodic state (i.e., ferri, anti-ferro, sine-wave, etc.). Thus the equation (2.32) indicates the change in free energy when the magnetic structure is altered.

The absolute value of μ is used in the first term on the left because, at higher temperatures (i.e. in the sinusoidal region), the applied field, if above the critical field, does not force immediate saturation. In this sinusoidal region then $\langle\ \mu\ \rangle_\lambda = 0$ and $\langle\ |\ \mu\ |\ \rangle_\lambda = \alpha\ \sigma\ (0)$. (2.33)

and the free energy will go as $\sigma^2(T)$ assuming sufficiently low temperature to neglect entropy.

Hence

$$H_c\ \alpha\ \frac{\phi^2\ (T)\ \sigma^2(0)}{\phi\ (T)\ \sigma\ (0)}\ , \tag{2.34}$$

and

$$H_c \propto \frac{\phi^2(T)}{\phi(T)} \quad . \tag{2.35}$$

For rare earth metals there is always an excess magnetization observed which is above that as given by equation (2.19). This can be attributed to polarization of the conduction electrons (equation 2.29)). This shows up as a spontaneous magnetization superposed upon the spontaneous magnetization arising from the ions. It might be argued that an "internal" polarizing field acts on the conduction electrons to produce a spontaneous magnetization. This "internal" field can be determined by noting the change in magnetization above saturation caused by an applied field. Hence,

$$\frac{\sigma_{e,o}(T)}{\text{"H"}} = \frac{\sigma_{e,\ Ha}(T) - \sigma_{e,o}(T)}{Ha} \quad . \tag{2.36}$$

Here $\sigma_{e,o}(T)$ is the spontaneous electronic magnetization at temperature T, $\sigma_{e,\ Ha}(T)$ is the electronic magnetization at T, "H" is the "internal" polarizing field, and Ha is the applied magnetic field intensity.

Then

$$\text{"H"} = \sigma_{e,o}(T) \ / \ \chi_{hf}(T) \ . \tag{2.37}$$

Where

$$\chi_{hf}(T) = \frac{\sigma_{e,\ Ha}(T) - \sigma_{e,o}(T)}{Ha} \tag{2.38}$$

is the high field magnetic rusuplibility per gram. Now if the material is ferromagnetic and at $4.2^{o}K$

$$\chi_{hf}(4.2^{o}) \simeq \chi_{hf}(0^{o}) \ . \tag{2.39}$$

III. EXPERIMENTAL PROCEDURE

The basic method of measuring magnetizations was to vibrate a magnetized sample inside a number of coils in which case the magnetic moment is proportional to the voltage induced in the coils. The two approaches to measurements can be called for convenience the "single" Foner method and the "double" Foner method. Both methods are more or less similar to the method as described by Foner (31).

A. The Single Foner Method

1. Design of the magnetometer

The magnetometer was of the vibrating sample type. The sample was oscillated in a homogeneous magnetic field at the center of a pick-up coil system. The voltage induced in the pick-up coil system was then compared with a reference signal which has the same frequency and phase as the sample signal. This comparison (or ratio) will be dependent on the total moment of the magnetized sample. General construction details are shown in Figure 1.

The sample was attached to a long balsa-quartz rod, hereafter called the sample rod, which was driven by a Ling vibrator at 102.5 cps. The sample rod passes through and was lightly attached to the voice coil of a high quality radio speaker so as to generate a reference voltage. The rod then extended the length of the dewar system where it ended with a teflon spacer just above the sample which was in turn centered at the solenoid field center.

The vibrator and reference speaker were housed in a vacuum-tight chamber which was mounted on a compound vice table. The vice table could be moved horizontally both laterally and longitudinally to allow for hori-

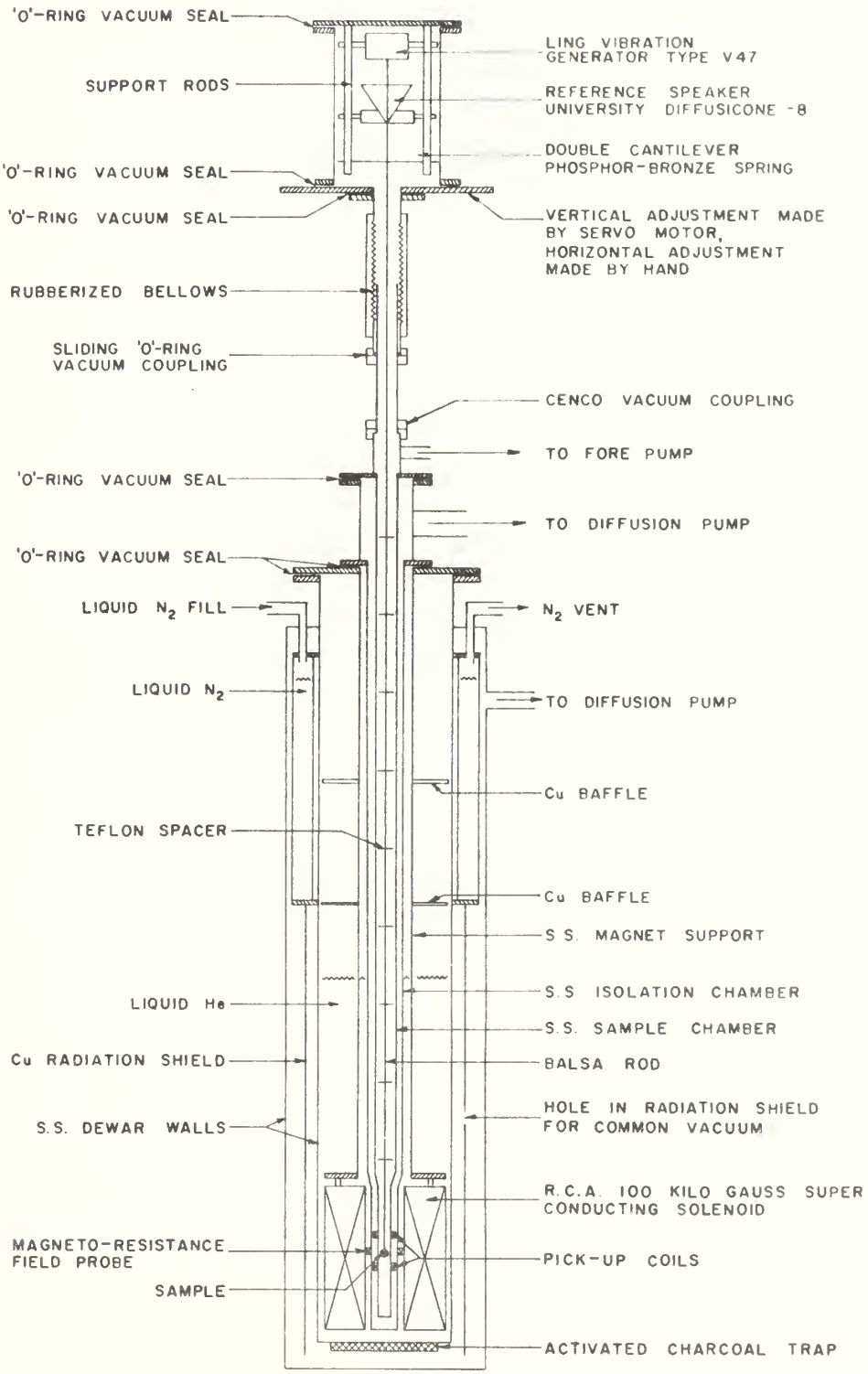

Figure 1. The general construction of the single Foner magnetometer

zontal centering. The chamber was also linked to a servo motor assembly which allowed for vertical centering.

Extending below the vibrator chamber were a set of rubberized bellows which acted as a horizontally flexible coupling so as to permit horizontal centering movements. Attached to the lower end of the rubberized bellows was a sliding "O" ring seal within which slid a chrome plated stainless steel tube. This arrangement allowed for vertical freedom of movement. This stainless steel tube was then cenco fitted to the upper end of the dewar system.

The sample rod itself was balsa with a quartz tube extension attached to the lower end. Balsa is light and has favorable damping properties which prevent standing waves from forming down the sample rod. The Balsa rod was coated with a low viscosity epoxy to prevent moisture absorption and tapered from top to bottom. The quartz tube extension was evacuated by means of a small line drilled through the balsa rod and was epoxied to the balsa rod with Armstrong C-7. The teflon spacer was epoxied to the outside lower end of the quartz rod. Into the lower opening of the quartz rod was epoxied a phenolic plug tapped for a 2 x 56 screw. A 2 x 56 screw-nut assembly threaded into this phenolic plug to act as the sample holder. (See Figure 2).

The sample vibrated inside a pyrex tail (see Figure 3), upon which were wound the pick-up coils, sample temperature thermocouple, heater control thermocouple, and the heater.

It was very important that the pick-up coils be wound so as to prevent any voltage being induced by changes in the applied field. The cylindrical symmetry of the solenoid facilitated this by allowing us to locate the pick-up coils symmetrically about the magnetic field center. The coils

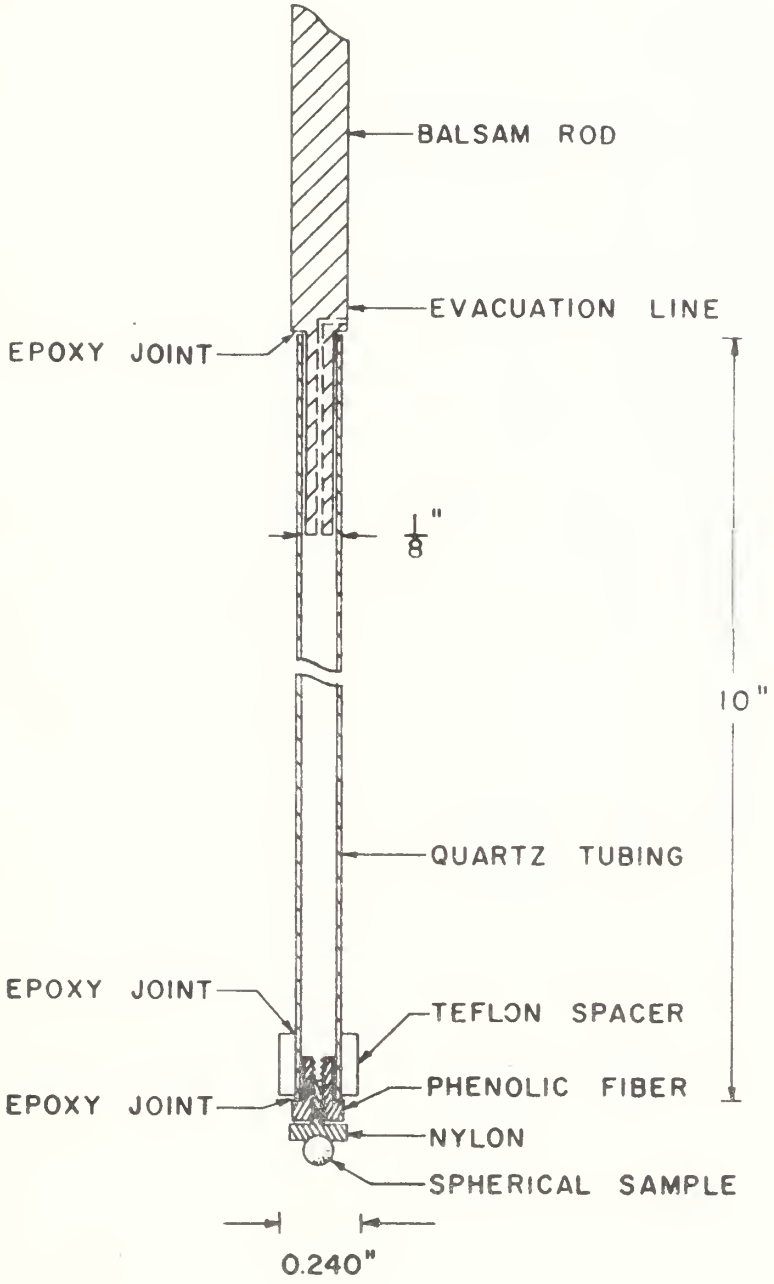

Figure 2. The sample holder used in the single Foner method.

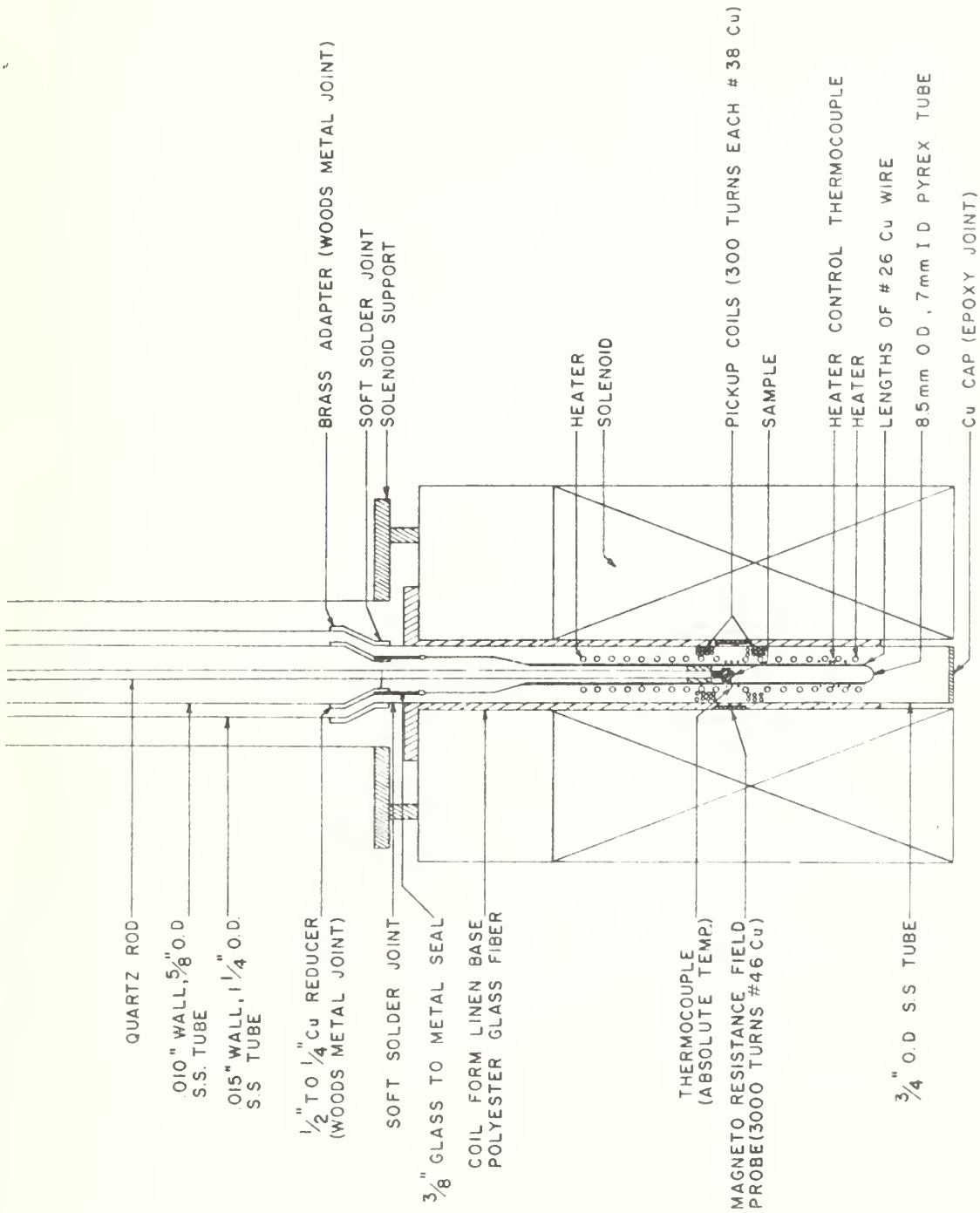

Figure 3. Construction details in the solenoid for the single Foner magnetometer.

were then wired in series-opposition.

Both the sample thermocouple and the heater control thermocouple were three wire junctions of copper, constantan, and gold-iron. Above 35° K, a copper versus constantan thermocouple was used. Below 35° K a copper versus gold-iron thermocouple was used. The composition of the gold-iron wire was 0.03% iron. This composition showed no dependence upon applied magnetic field (7). The gold-iron wire was calibrated against a known germanium resistor. The constantan wire calibration was that as given by Powell et al. (32).

Both thermocouples were normalized to the calibration curves according to the system as described by Rhyne (33). The absolute thermocouples were read with a Leeds and Northrup type K-3 potentiometer and null detector.

The sample temperature thermocouple was mounted on the pyrex tail opposite the sample. In order to insure a legitimate estimate of sample temperature, helium exchange gas at low pressure (about 75 microns of mercury) was kept in the sample chamber to give good thermal contact between the sample and the thermocouple. This method results in an accuracy for reading sample temperature of $\pm$ 0.5° K.

The heater consisted of No. 38 manganin wire wound astatically on the pyrex tail. An open space (about 3/4") was left opposite the sample to allow the sample temperature thermocouple to be anchored there. The heater control thermocouples were anchored beneath the heater winding to give a fast response time. It was discovered that the glass tail alone would not conduct heat rapidly enough to control properly. Therefore, it was necessary to lay strips of copper wire on the outside of the pyrex tube to give adequate thermal conduction along the tail. The heater control thermocouples were read with a Rubicon type K-2 potentiometer. The desired

emf was preset on the Rubicon potentiometer and an error voltage read by A Keithley model 153 microvoltmeter. The output from the Keithley was fed into a temperature control amplifier and power supply as described by Rhyne (33). Temperature could be controlled within $\pm$ 0.2° K.

The applied magnetic field was determined by measuring the magnetoresistance of a high purity copper coil. The coil was wound astatically of 3000 turns of No. 46 wire on a form manufactured of glass base polyester fiber. This form was slipped into place inside the 1.01 inch bore of the solenoid.

The magnetoresistance was determined by means of the four probe method. The current was supplied by a pack of mercury cells and was measured by reading the voltage across a 10 ohm standard resistor with a Leeds and Northrup K-3 potentiometer and null detector. The current was then adjusted to 1 milliampere. Then the voltage was measured by the same K-3 potentiometer, thereby giving the magnetoresistance.

The magnetoresistance field probe was calibrated against a small probe of high purity copper wire (99.999%) made by Sigmund Cohn Corporation. This small probe was calibrated against an N.M.R. gaussmeter in a high homogeneity 60 kilo-Oersted solenoid. Above 4 kilo-Oersted, the resistance of this probe was linear with field, and is assumed to remain so up to 100 kilo-Oersted. The magnetic field is read to the nearest 100 Oersted. The overall accuracy of field measurement is estimated to be $\pm$ 0.5%.

The applied field was produced by a solenoid wound with Nb_3Sn superconductive ribbon. The solenoid has a maximum rated magnetic field of 100 kilo-Oersteds. It is characteristic of superconductive solenoids that they show "magnetic images", that is, a ring of magnetic dipoles forms on the superconductive ribbon which moves in phase with the vibrating

sample. It is this effect that was the most troublesome for accurate magnetometer design.

The sample signal pick-up coils were one of two source inputs which make up an AC bridge network (Figure 4). The other source input was the reference voltage. Because eddy currents were formed in the sample, the pick-up coils, and even in the superconductive ribbon, there was a component voltage called quadrature detected by the pick-up coils which was 90^{o} out of phase with the reference signal. In order to get true readings of the sample signal this quadrature had to be subtracted from the bridge circuit.

The reference speaker had an impedence of 8 ohms. So for proper power transfer, the reference signal was fed into a resistive load of 10 ohms (a 9 ohm and 1 ohm resistor in series). The reference voltage was taken across the 1 ohm resistor. This voltage passed through a high quality isolation transformer (Gertsch, model ST248B) and then into a Gertsch ratio transformer model 1011. The output from the ratio transformer was used to null the in-phase component of the sample pick-up coils.

The quadrature subtract voltage was generated by placing a high impedence capacitor in series with a variable resistor across the reference loudspeaker. The high capacitive reactance resulted in a voltage across the variable resistor which is 90^{o} out of phase with the reference voltage. This subtracted out the quadrature.

The bridge circuit impedence was a maximum of 150 ohms and usually nearer to 100 ohms. The input impedence of the phase sensitive amplifier was larger than a megaohm. Hence a matching transformer of turns ratio 100:1 was used.

The phase sensitive amplifier was a high gain, narrow band amplifier

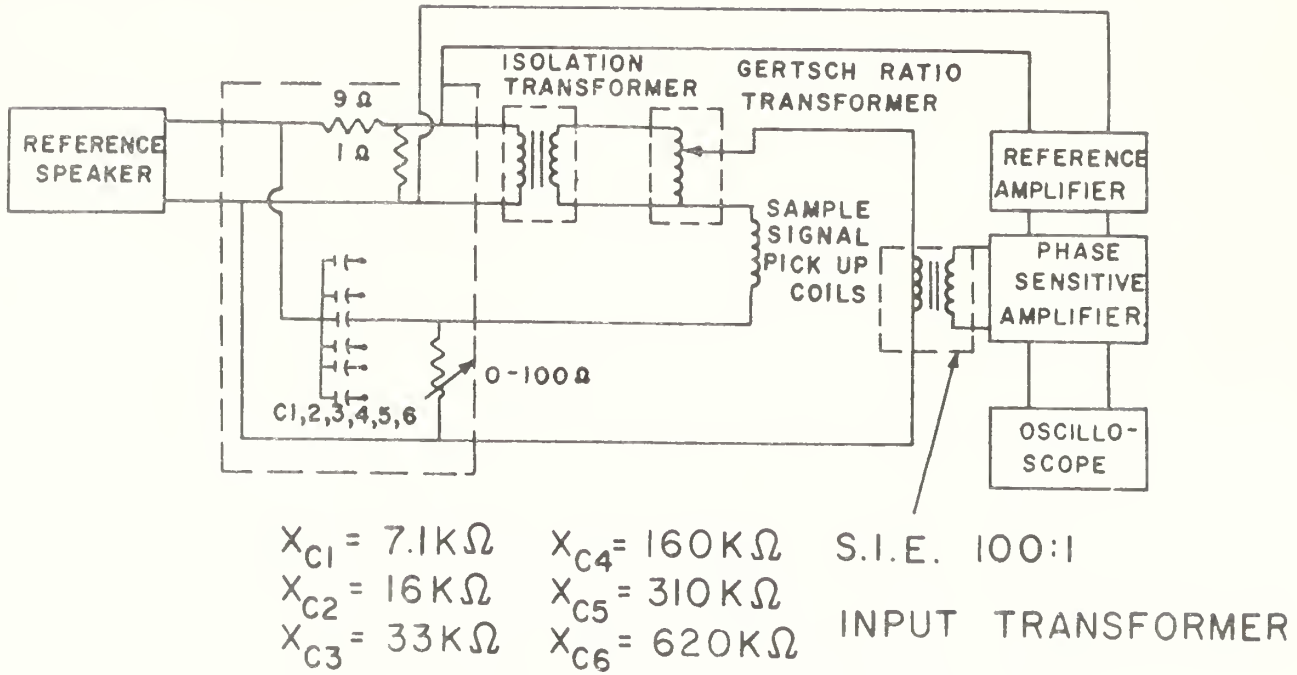

Figure 4. The AC bridge network used in single Foner magnetization measurements.

followed by a phase sensitive detector with unity gain. The output from the phase sensitive detector was D.C. and was displayed by a meter on the front panel, and on a Tektronix type 531A oscilloscope.

The phase sensitive amplifier required an input voltage of 1 volt at frequency equal to the signal of interest, and of necessity it had to be of the same phase relationship relative to the signal to be detected. This was accomplished by taking the voltage across the 1 ohm resistor, amplifying it with a low gain, high input impedence (1 megaohm) amplifier. To avoid ground looping, the output of the amplifier was transformer isolated before being fed into the phase sensitive amplifier.

Before taking a Gertsch ratio transformer reading the procedure was as follows:

1. Null out the quadrature by adjusting the variable capacitors and the variable resistor to get a minimum signal on the oscilloscope. This process was repeated until the most sensitive signals are minimized.
2. Set the Gertsch ratio transformer to get a null on the scope and phase sensitive amplifier.
3. Center the sample horizontally and vertically by maximizing the signal on the phase sensitive amplifier.

It was sometimes necessary to repeat the above procedure one or more times to get the proper null signal; but usually, after the initial centering following placement of the sample rod in the solenoid, only small adjustments were needed.

2. Magnetization measurements

The magnetization per gram was determined by using the equation

$$\sigma_x\ (Ha,\ T) = \frac{m_{Fe}\ G_x(H_a,\ T)F(T)}{m_x\ G_{Fe}(H_a, T)F(T')}\ \sigma_{Fe}(H_a,\ T')\ . \qquad (3.1)$$

where m_{Fe} and m_x are the weights of the samples. $G_x(H_a,\ T)$ is the Gertsch ratio reading for the unknown at applied field H_a and temperature T $G_{Fe}(H_a,\ T')$ is the Gertsch ratio reading for iron at the same applied field H_a and temperature T'. σ_x and σ_{Fe} are the magnetization per gram of the unknown and iron. F(T) and F(T') are known temperature correction factors.

The value of the saturation of the magnetization of iron $\sigma_{Fe}(H_a,\ T')$ at various temperatures was determined using data from 4.2 K to 140 K reported by Argyle et al. (34) and an accurate point at 288 K reported by Danan (35, 36) and fitting a smooth curve through them.

It is known that iron does have a susceptibility above saturation; however, there is some disagreement over its size (37, 38). Therefore the iron susceptibilities were set at saturation values over the whole range of applied field. When more accurate information is reported the data can be corrected. Neglecting the iron high field susceptibility would cause a maximum 1/2% error at 100 kilo-Oersteds.

The temperature correction factors, F(T), were due to the thermal expansion of the pick-up coils and amount to a 1% correction when corrections are made from 300 K to 4.2 K.

The iron Gertsch ratio value was obtained by running several isotherms with iron in the magnetometer until the values obtained reproduced within 0.2%. This process was necessary because of the Nb_3Sn ribbon formed dipole images of the sample which feed back through the AC bridge system. The process was further complicated by the fact that the image behavior was strongly dependent on the history of the solenoid. That is, strong

current vorticies were set up in the ribbon which did not remain constant with each sweep over the entire range of applied magnetic field. The strength of these vorticies can be gauged by noting that after sweeping from zero current to full field and back to zero current there was a residual field of about 6 kilo-Oersteds. These images were also very unstable following a quench and consequently, after a quench, it was necessary to warm the dewar system to room temperature before operating again. In any event, the images were instrumental in giving an overall accuracy of $\pm$ 2% to the magnetometer and a relative accuracy of $\pm$ 0.2% for a single given isotherm.

The procedure for obtaining the magnetization was to first get the calibration Gertsch ratio readings for iron as previously noted and then to replace the iron with the unknown. The data were then taken either as isotherms or isofields giving a raw susceptibility $\sigma_x(H_a, T)$. This figure had to be corrected for demagnetization according to the equation

$$H_{int} = H_a - Nd\,\sigma_x(H_a, T) , \qquad (3.2)$$

where H_{int} is the internal magnetic field intensity, d is the density and N is the demagnetizing factor obtained from Bozorth (39). In this manner the data was converted to $\sigma_x(H_{int}, T)$.

3. Sample preparation

The rare earth metals were produced at the Ames Laboratory by an ion exchange process (40) which separates each from the remaining rare earth metals. The metal was then arc-melted onto a cold copper hearth which forms large thermal strains in the resultant button. These strains nucleate the grain growth when the button is annealed at a temperature just below melting. The process is described in more detail by Nigh (41). The

gadolinium, dysprosium, and terbium crystals were grown by Dr. R. W. Williams, the holmium crystals by Dr. L. R. Sill, and the thulium crystals in a modification of Nigh's process by Dr. L. R. Edwards (42).

For the single Foner system as described here, spherical samples were prepared and mounted as described by Richards (7).

B. The Double Foner Method

1. The general design

The double Foner method utilized a dual set of pick-up coils located symmetrically about the field center. A sample holder containing two samples was vibrated inside these coils. The two samples were each surrounded by current carrying trimming coils mounted on the sample holder which acted to subtract from or to enhance the sample magnetic moments. When the dual set of pick-up coils saw identical apparent magnetic moments, a null signal resulted. Except for the region of the solenoid, general construction details were the same as that shown in Figure 1.

The sample rod was made entirely of balsa. Into the lower end of the sample rod was epoxied a 4 x 40 headless nylon screw. The sample holder (Figure 5) was then threaded onto this screw.

The sample holder was manufactured of nylon. It consisted of two exterior coil forms with a hole drilled through the center. The coil forms carried the trimming coils which were wired in series opposition. The samples were placed inside the trimming coils with nylon spacers acting to insure that each sample was centered in its respective trimming coil. The samples and spacers were held in place by a 6 x 32 nylon screw which threaded into the lower end of the sample holder.

The dual set of pick-up coils was mounted on an open-ended pyrex

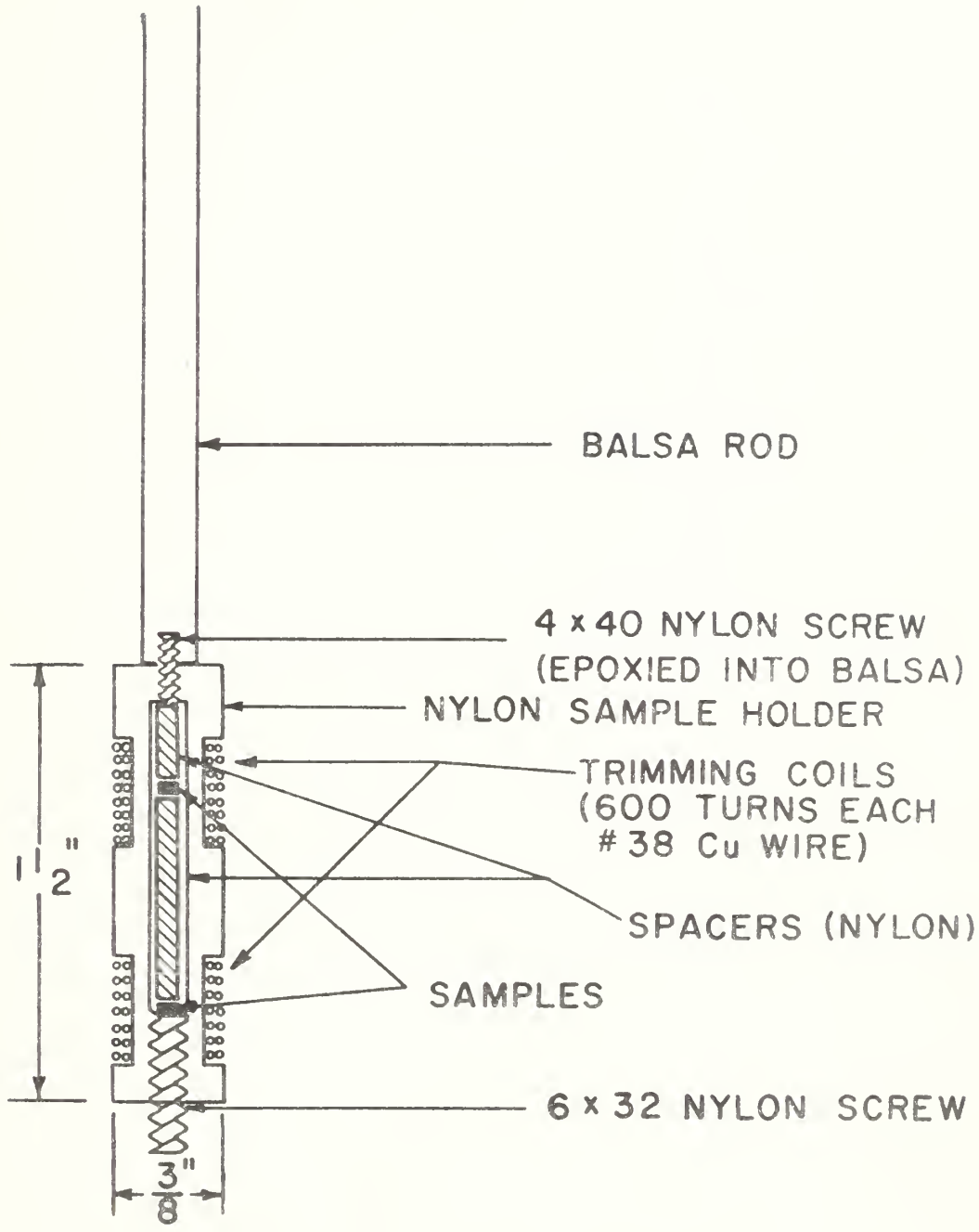

Figure 5. The sample holder used in double Foner measurements.

tube extending into the bore of the solenoid (see Figure 6). Thus the pick-up coils and the sample holder were in the liquid helium bath. The dual set of pick-up coils was symmetrically placed around the field center.

The pick-up coils were wired as shown in Figure 7. This wiring scheme, as compared to others, gave the maximum error signal when the two apparent moments were unequal. In addition, this wiring scheme was astatic to changes in applied field.

The signal from the pick-up coils was fed into an A-C bridge (Figure 8). The bridge had the same components as the one described in the single Foner method except that the Gertsch ratio transformer was omitted.

The current for the trimming coils was supplied by a high stability current supply having a range of 60 to 1000 milliamperes, or by a current source using a Willard cell having a range of 0 to 150 milliamperes. The current was determined by reading the voltage across a 1 ohm standard resistor with a Leeds and Northrup K-3 potentiometer and null detector. For either current supply, stability was better than 0.1%.

The applied field was measured as described earlier for the single Foner system. Prior to operating the system, centering was accomplished by putting a constant current through the trimming coils while the sample chambers were empty and recording the Gertsch ratio values obtained using the bridge circuit for the single Foner method. When the trimming coils were centered with respect to the pick-up coils a maximum was obtained from the Gertsch ratio transformer.

2. Sample preparation

The samples were cut from single crystals aligned by Laue back reflection of X-rays by a Sparcatron spark machining apparatus. They were cut into cylinders along the desired axis by using a hollow tantalum rod

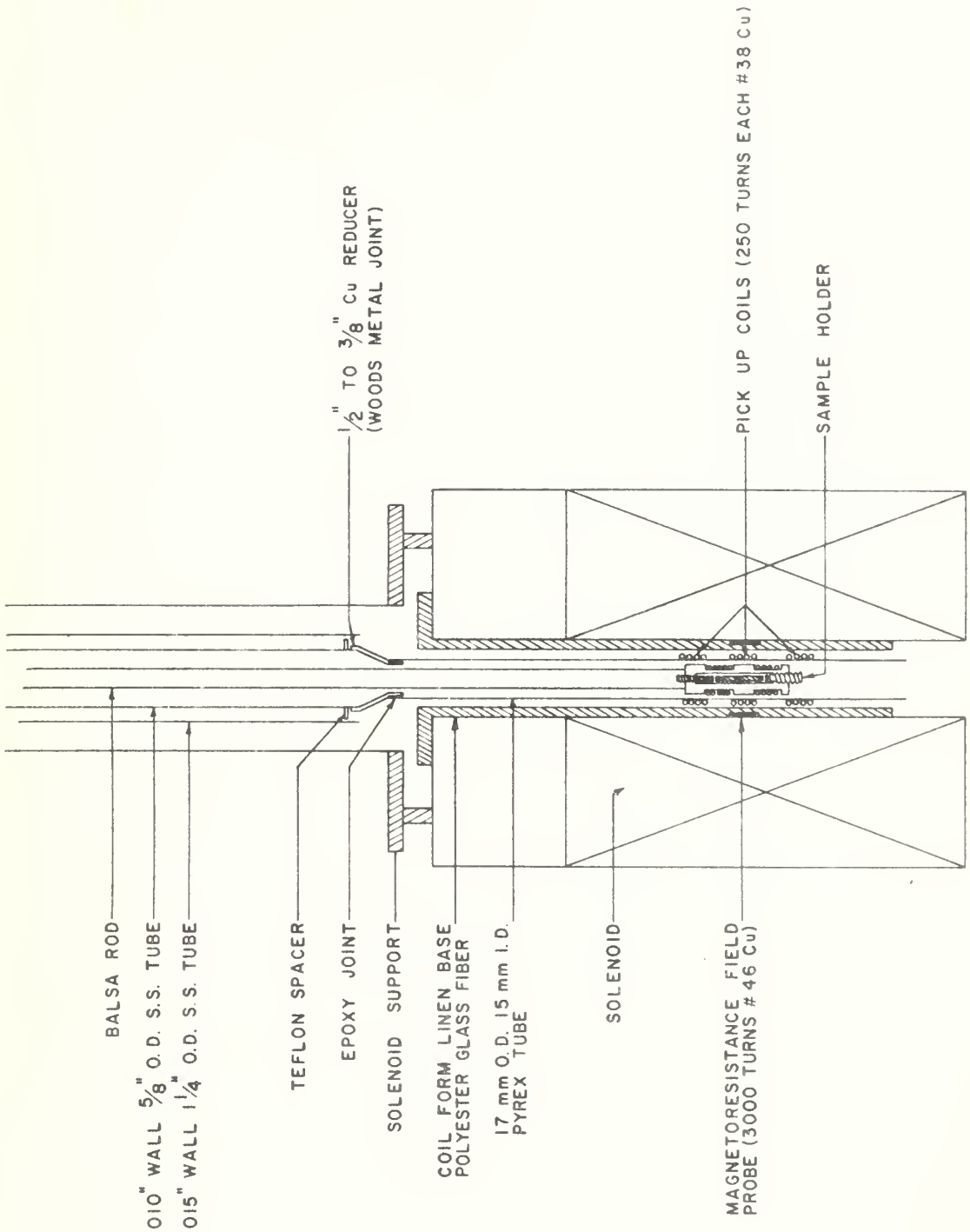

Figure 6. Construction details in the solenoid for the double Foner magnetometer.

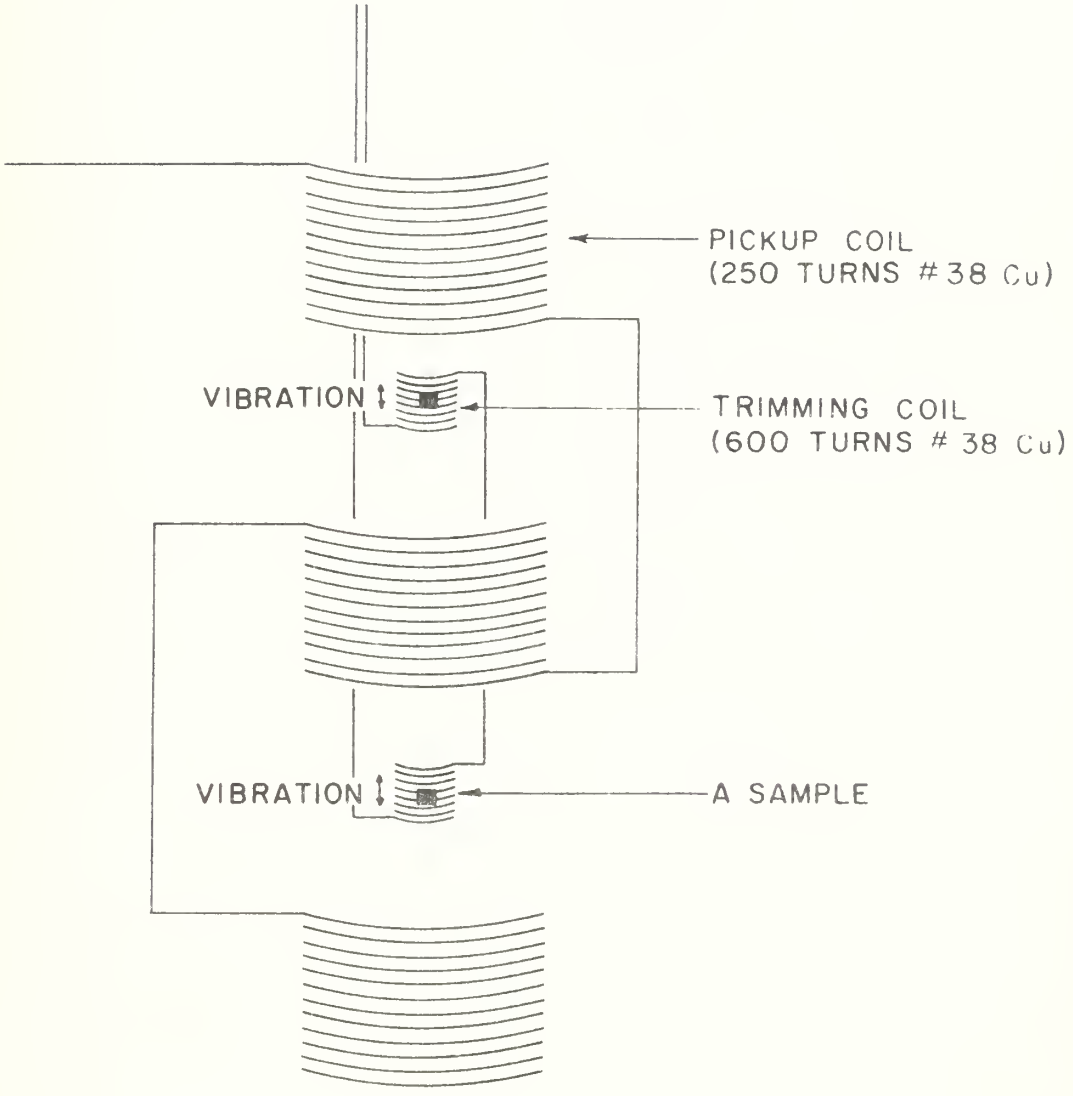

Figure 7. Wiring diagram for the pick-up coil in the double Foner method.

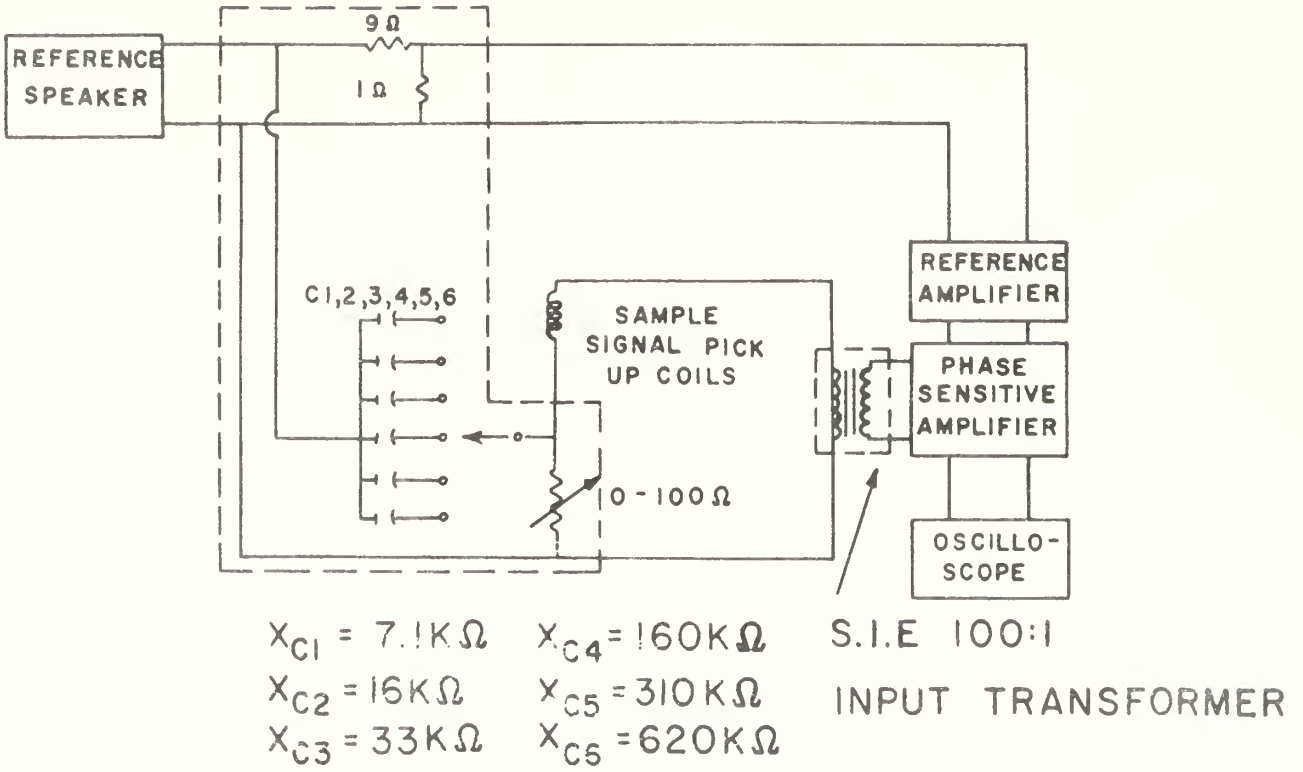

Figure 8. The AC bridge network used in double Foner magnetization measurements.

as the cutting tool. The samples were then hand lapped to the proper length, electropolished, and weighed. The crystals came from the same buttons as reported for the single Foner method.

3. Magnetization measurements

Magnetization measurements were made by using the equation

$$\sigma_x(4.2^o,\ H_a) = \frac{m_{Fe}\ \sigma_{Fe}(4.2^o,\ H_a) + \Delta M}{m_x} \quad . \tag{3.3}$$

where $\sigma_x(4.2^o,\ H_a)$ and $\sigma_{Fe}(4.2^o,\ H_a)$ are the magnetizations per gram of the unknown and the iron; m_x and m_{Fe} are the masses of the unknown and the iron samples. ΔM was the moment difference supplied by the trimming coils.

The quantity ΔM was obtained from a calibration curve which was produced by placing iron samples of differing weights in the sample holder. The relation used was

$$\Delta M = \sigma_{Fe}(4.2^o,\ H_a)(m'_{Fe} - m^2_{Fe}) \quad . \tag{3.4}$$

The value for $\sigma_{Fe}(4.2^o,\ H_a)$ was obtained from the curve used in the single Foner method. ΔM was produced by the current flowing through the trimming coils. Hence a calibration curve of ΔM versus the current could be plotted.

It was thought that because of the magnetic symmetry (i.e. equal moments vibrating inside dual pick-up coils sets) of the system, the image dipole signals would cancel out in the pick-up coils. However, an even more perplexing phenomenon occurred as discussed below.

Two different pick-up coils arrangements were used. The first arrangement had the top and bottom pick-up coils with equal area turns, and the central coil with double the area turns. The calibration curve

for this arrangement is shown in Figure 9. As can be seen from the figure the calibration line gave a current of -45 milliamperes when $\Delta M = 0$. The theoretical intercept should have been 0 milliamperes when $\Delta M = 0$. This calibration plot also showed an unacceptable amount of scatter. Therefore another modification was tried.

The second arrangement had all three pick-up coils with equal area turns. The calibration curve for this arrangement is shown in Figure 10. As can be seen from the figure the calibration line gave a current of -262 milliamperes at $\Delta M = 0$. In order to check this result, an empty sample holder was placed in the magnetometer. The trimming coil current required to achieve a null with an empty sample holder was -4 milliamperes. This result was interpreted to mean that the two sample moments were setting up higher order (quadrapole) magnetic images in the superconductive ribbon. So once again the images proved to be the limiting factor.

Data were taken using the second arrangement of pick-up coils on gadolinium (Figure 11), terbium (Figure 12), dysprosium (Figure 13), holmium (Figure 14), and thulium (Figure 15). In every case the high field magnetic susceptibility is much greater than previous studies (2), (3), (4), (5), (7), have indicated. In addition the spontaneous saturation magnetization values are in error up to 10%. Using data for thulium taken by Richards (7) at high applied fields to check the calibration, it was found that the calibration curve had shifted to the right and had a less steep slope. This depressing fact was then interpreted to mean that once again the images were dependent on the past history of the superconductive ribbon.

Using a superconductive solenoid with a larger bore (about 5 to 6 inches) and carefully matching samples to give nearly identical total moments should make at least the single Foner method accurate to within

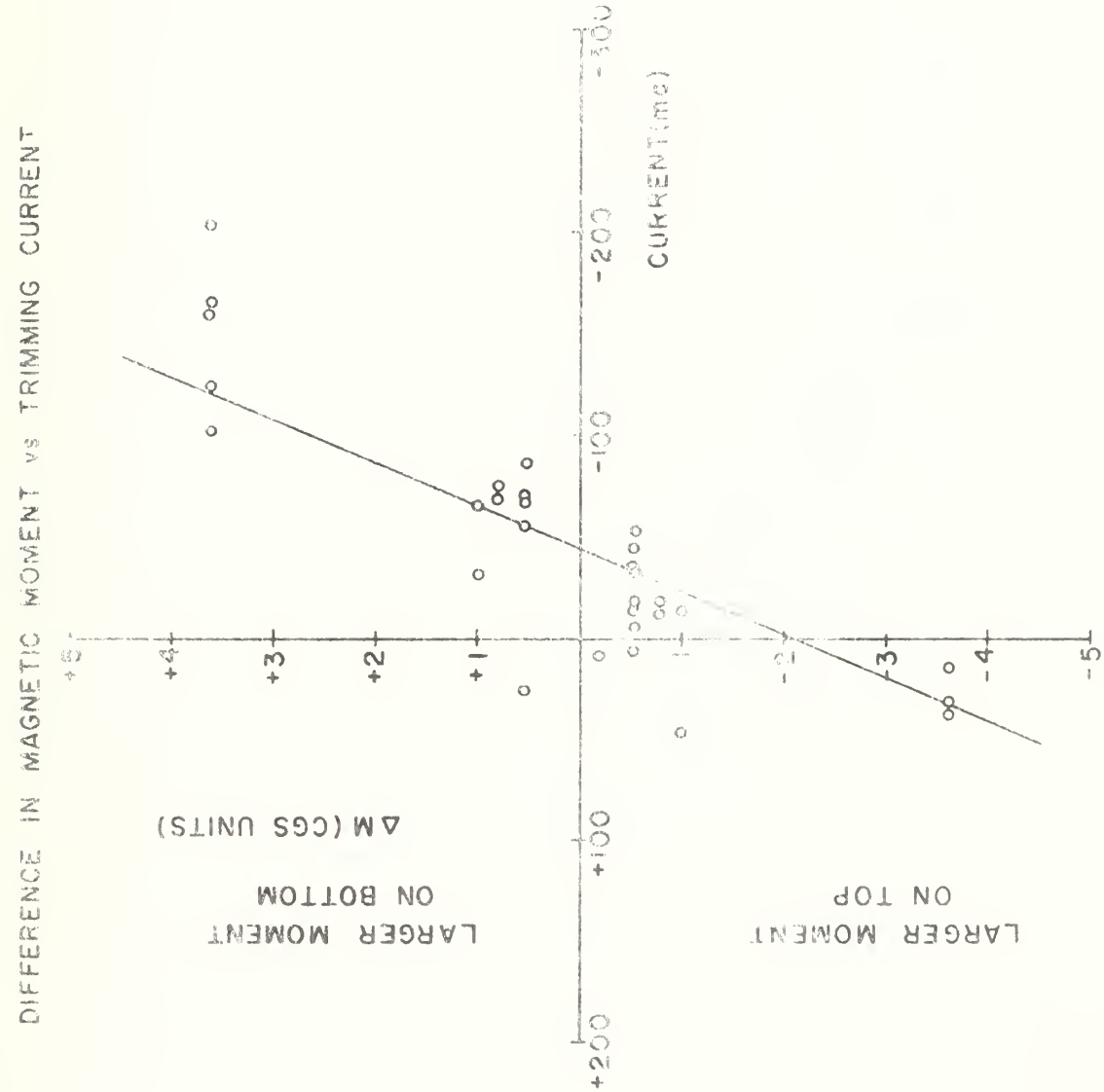

Figure 9. The calibration curve for the double Foner method with central coil having double the area turns.

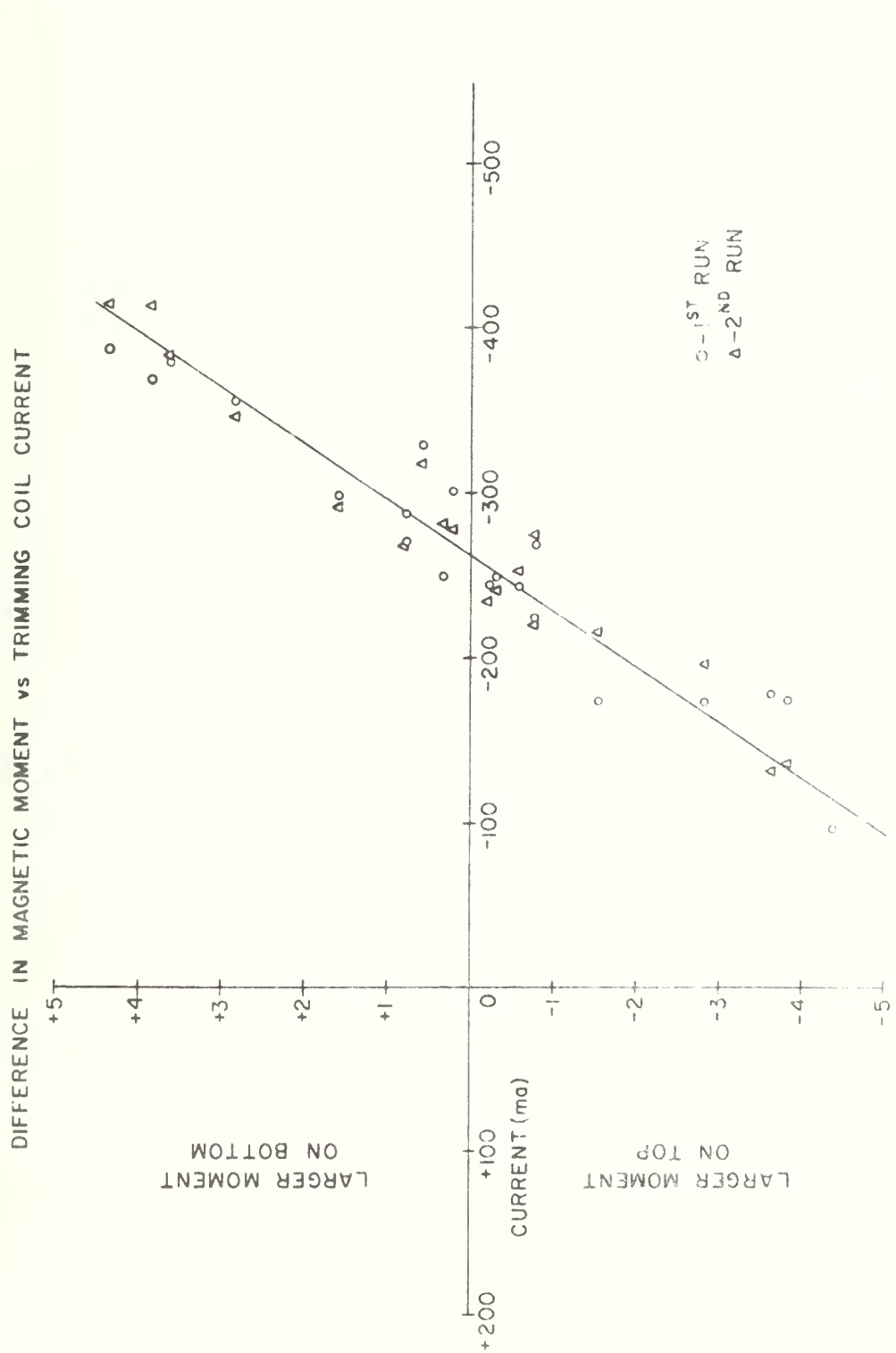

Figure 10. The calibration curve for the double Foner method with central coil having equal area turns.

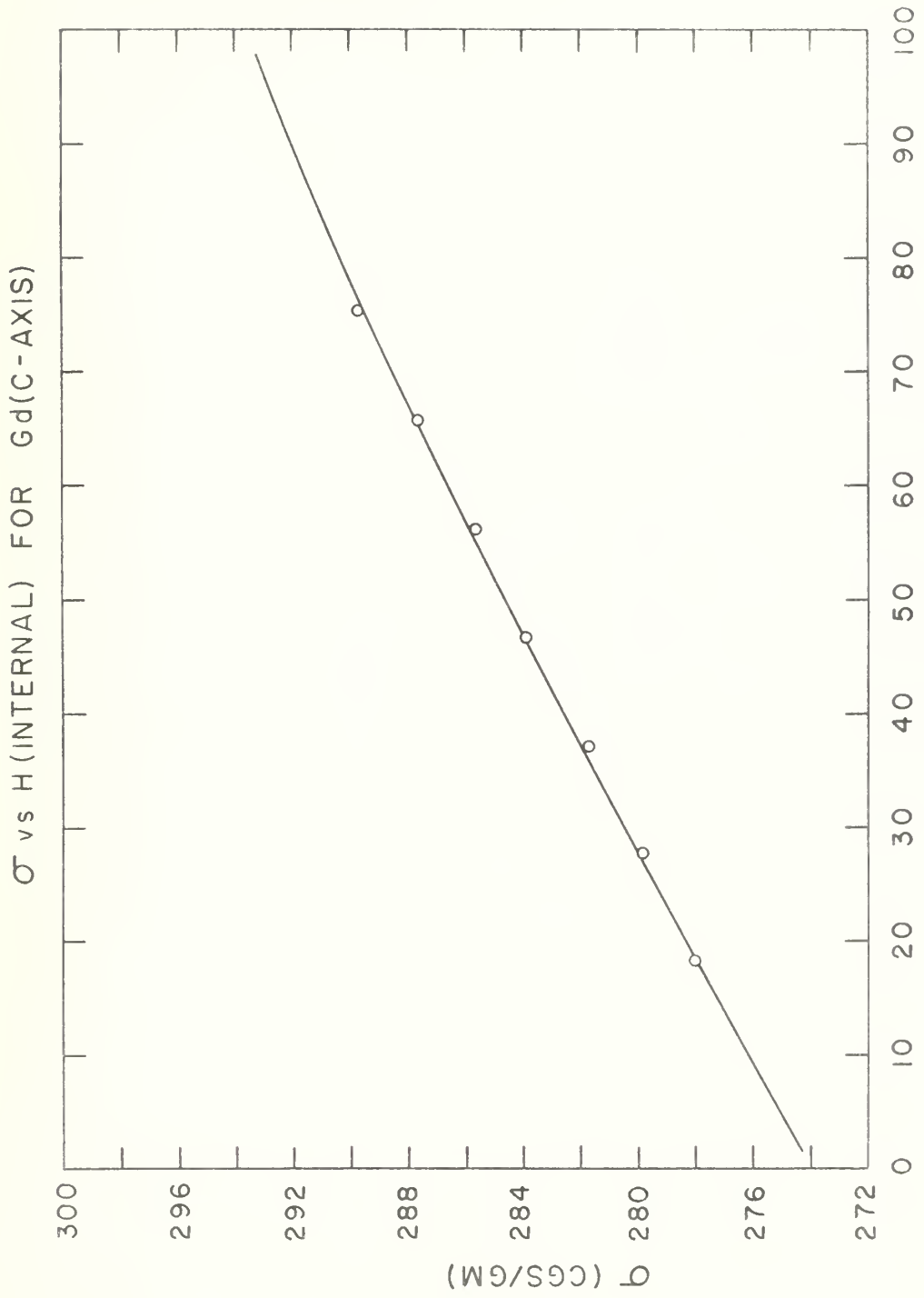

Figure 11. The magnetization as a function of internal field at 4.2 K for gadolinium.

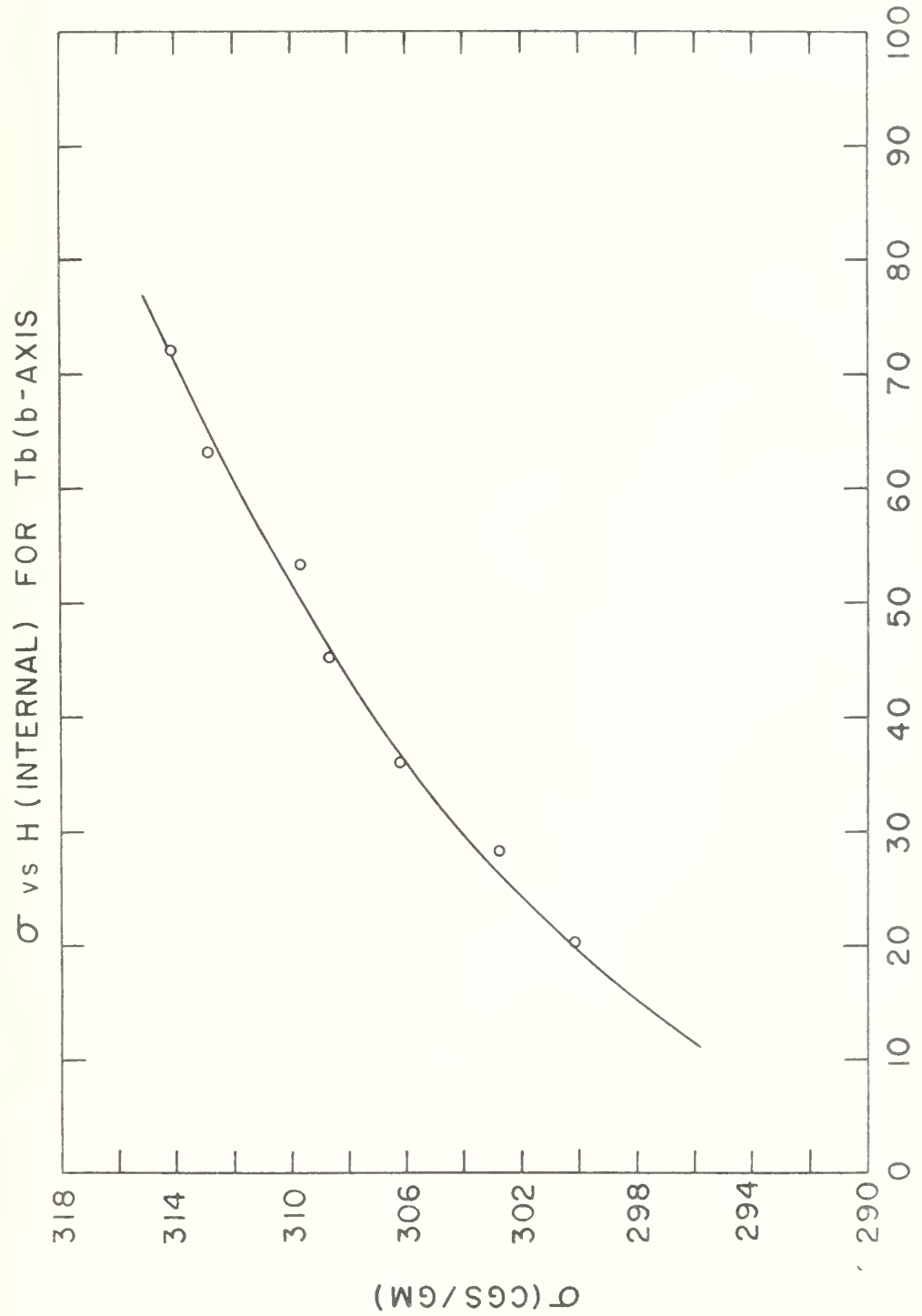

Figure 12. The magnetization as a function of internal field at 4.2 K for terbium.

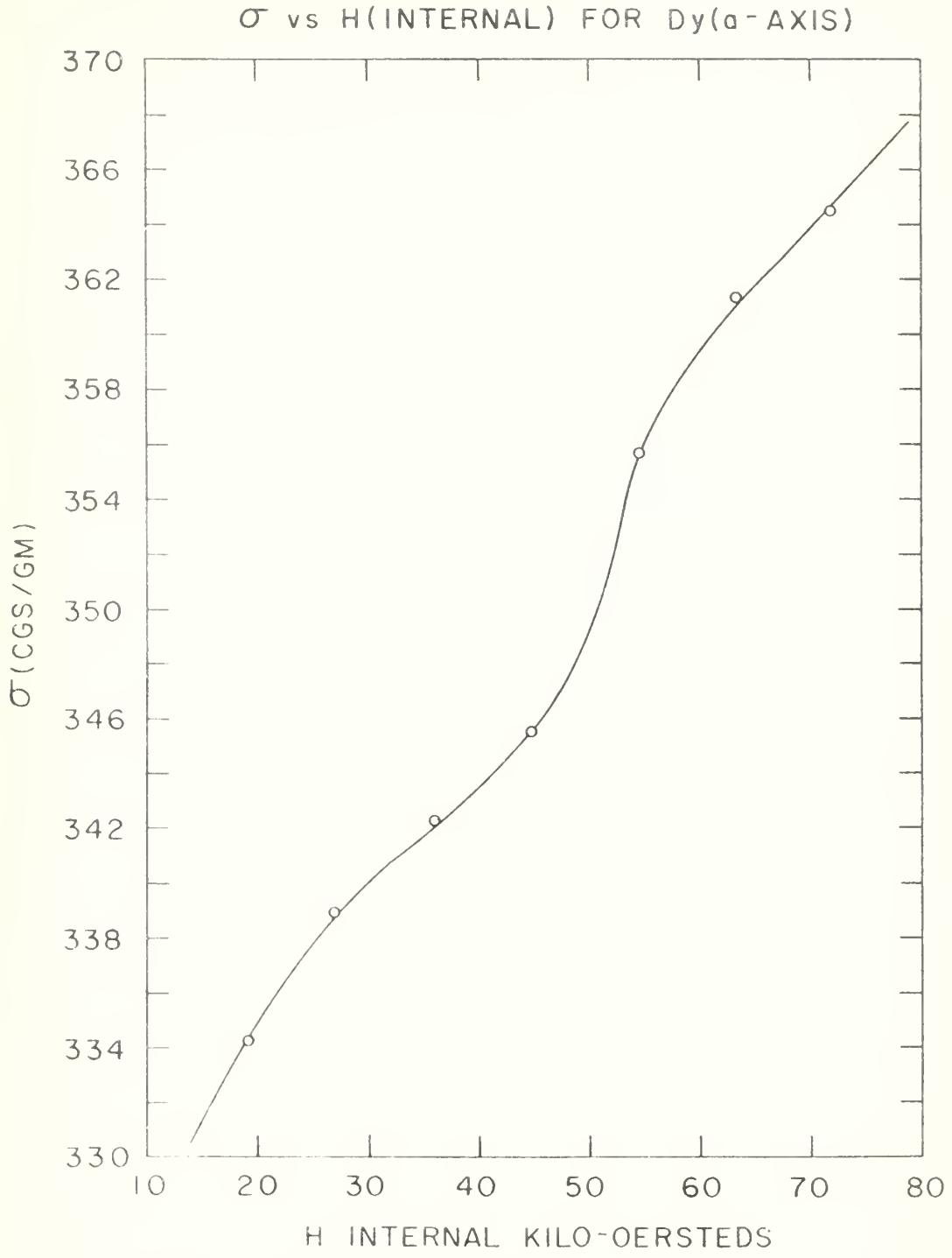

Figure 13. The magnetization as a function of internal field at 4.2 K for dysprosium.

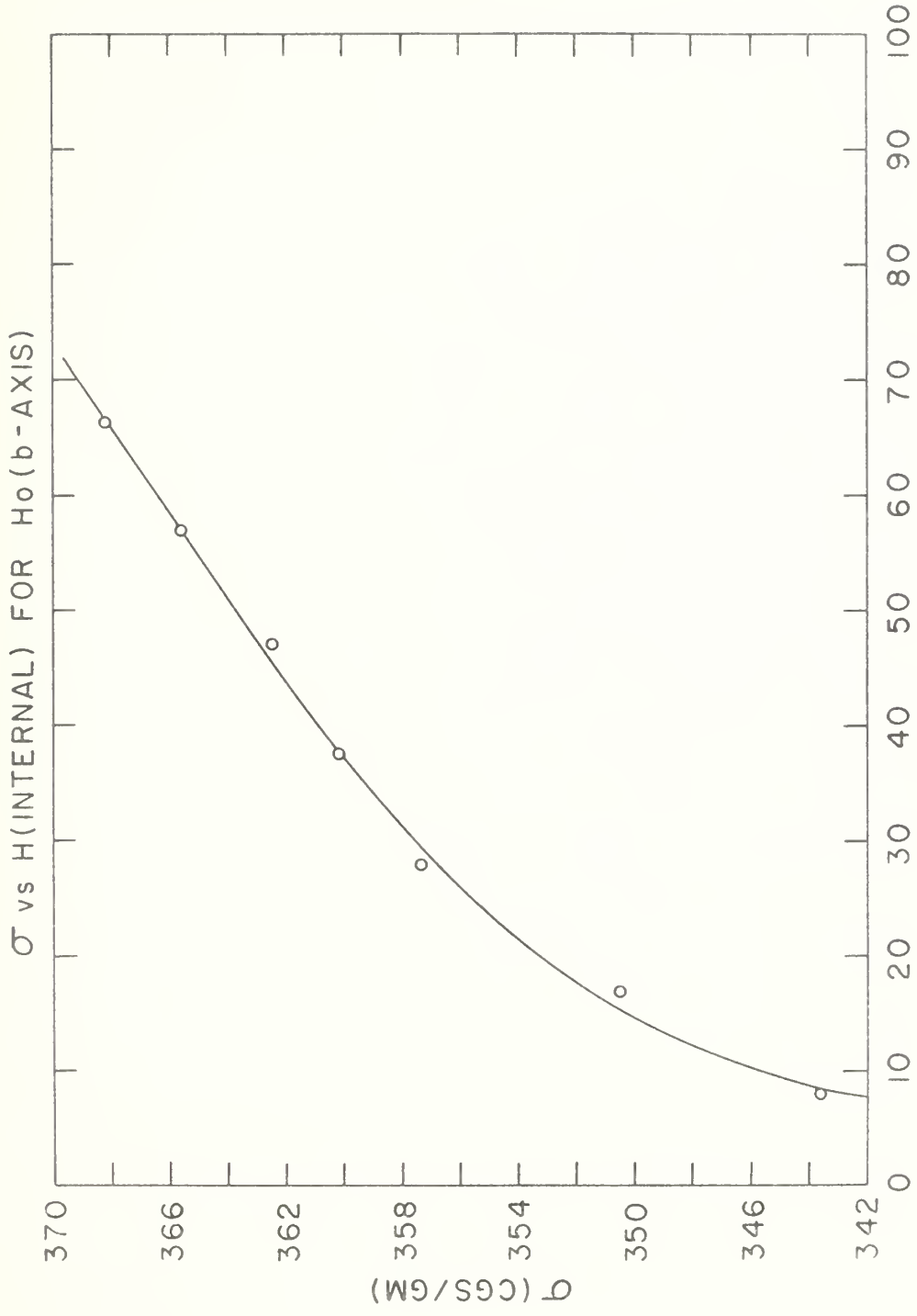

Figure 14. The magnetization as a function of internal field at 4.2 K for holmium.

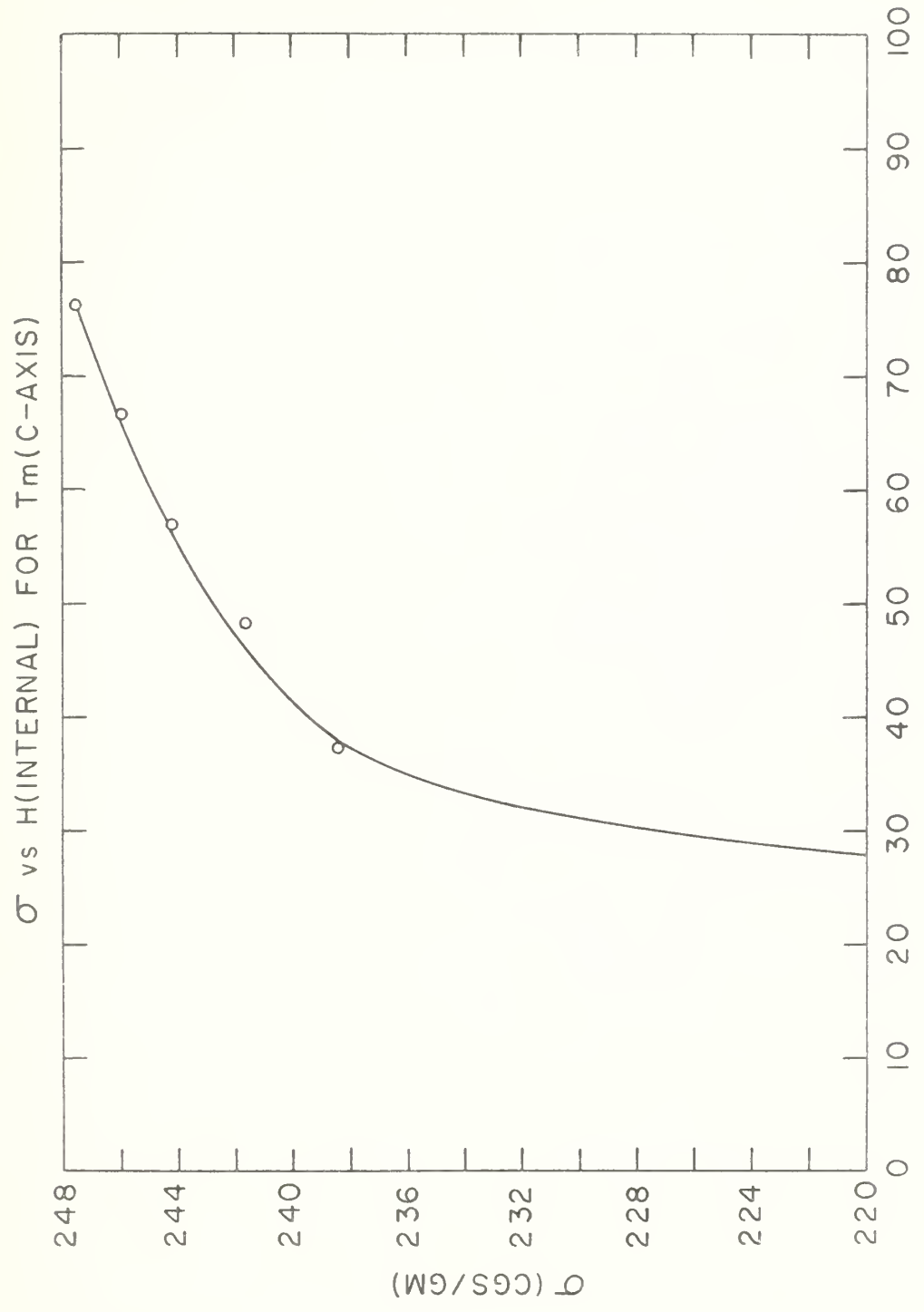

Figure 15. The magnetization as a function of internal field at 4.2 K for thulium.

$\pm$ 0.1% and might possibly make use of the double Foner method feasible to good accuracy. Additionally, elimination of the central coil might help mitigate some of the quadrupole contributions.

IV. RESULTS

The magnetization per gram for gadolinium and terbium was measured at 4.2 K and from 15 kilo-Oersted to 100 kilo-Oersted applied field by means of the single Foner method.

For gadolinium and terbium several isotherms each were taken. The spontaneous saturation magnetization was obtained by noting which isotherm had the most reproducable calibration curve (i.e. the calibration in which image drift was least) and using that isotherm's value for the spontaneous saturation magnetization. The remaining isotherm data were normalized to this value of spontaneous saturation magnetization.

The plot of σ_g versus H for gadolinium is shown in Figure 16. The spontaneous saturation magnetization, σ_o(4.2 K) was determined to be 265.9 emu/g which is 7.49 Bohr magnetons per atom. This compares with 7.39 Bohr magnetons per atom reported by Féron and Pauthenet (14). The high field magnetic susceptibility was found to be 3.3×10^{-5} emu/gOe as compared to 4.5×10^{-5} emu/gOe reported by Féron and Pauthenet (14). At 17.5 kilo-Oersted the plot gave 7.50 Bohr magnetons per atom as compared to 7.52 Bohr magnetons per atom as reported by Nigh (2).

The plot of σ_g versus H for terbium is shown in Figure 17. The spontaneous saturation magnetization was determined to be 326.1 emu/g which is 9.28 Bohr magnetons per atom. This is identical to the value as reported by Féron and Pauthenet (14). The high field magnetic susceptibility was found to be 7.3×10^{-5} emu/gOe as compared to 5.2×10^{-5} emu/gOe reported by Féron and Pauthenet (14). At 17.5 kilo-Oersteds, the plot gave 9.29 Bohr magnetons per atom as compared to 9.26 Bohr magnetons per atom reported by Hegland (3).

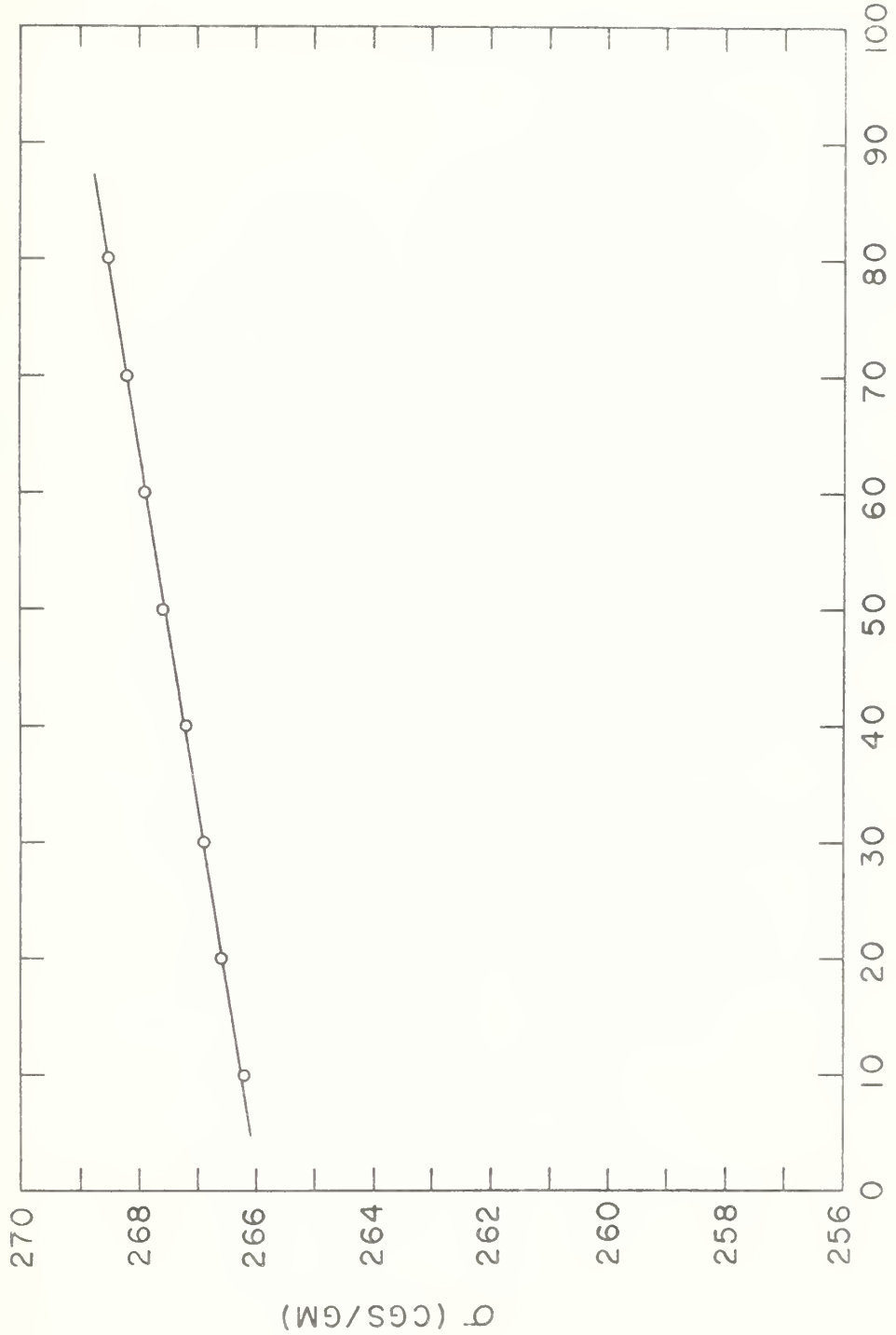

Figure 16. The magnetization as a function of internal field at 4.2 K for gadolinium.

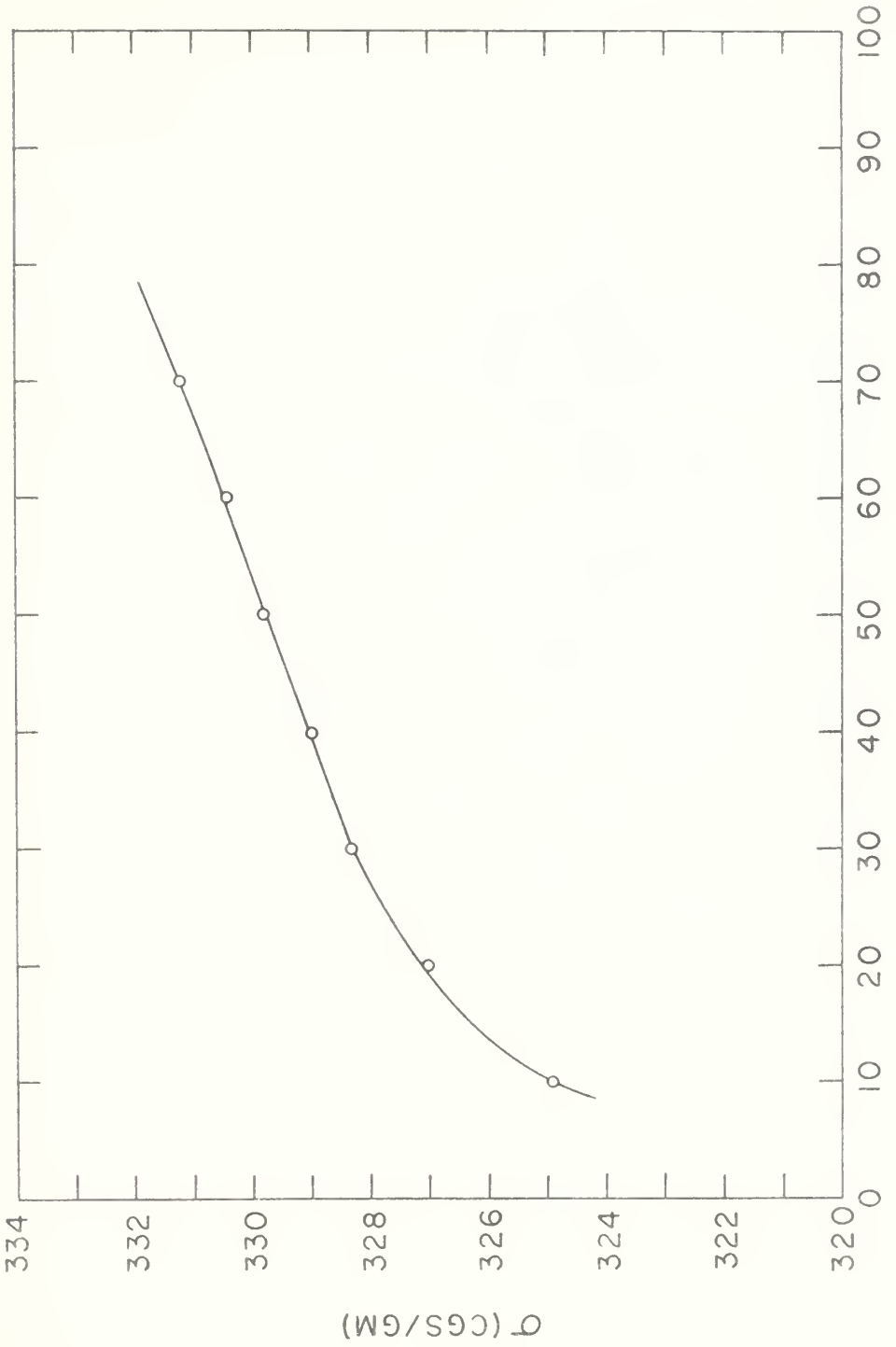

Figure 17. The magnetization as a function of internal field at 4.2 K for terbium.

Figure 18 shows the critical field as a function of temperature for holmium (b-axis). The curve is flat from 4.2 K to 12 K and rises steadily thereafter to 70 K. At 78 K holmium showed no critical field.

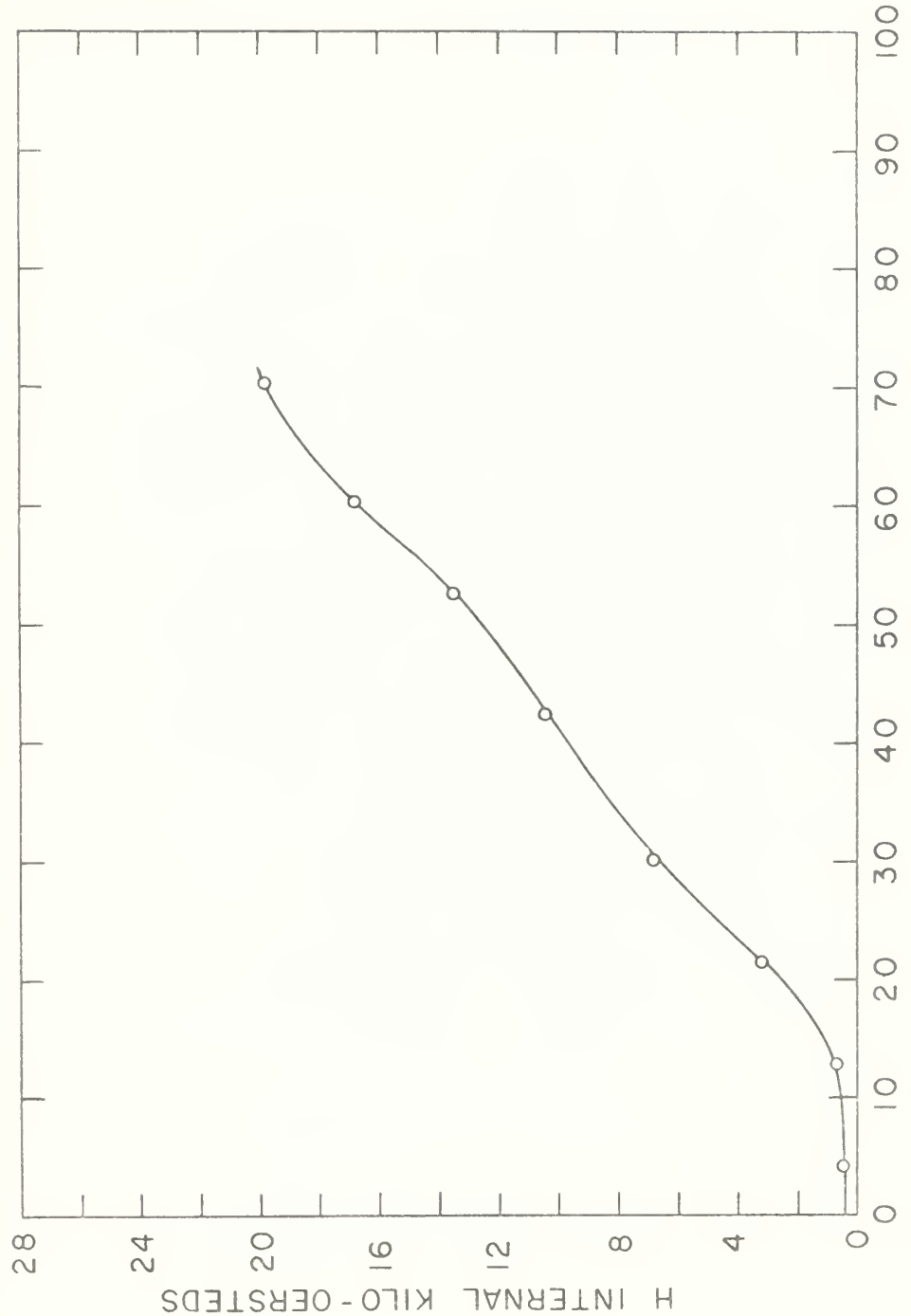

Figure 18. The critical field as a function of temperature for holmium.

V. DISCUSSION

By using equations (2.31) and (2.29) the density of electron states at the Fermi surface, $N(E_F)$, and the interaction energy, I, can be determined. The results of such a calculation gave $N(E_F) = 3.30 \times 10^{34}$/erg-cm^3 and $I = 1.26 \times 10^{-13}$ erg for gadolinium. This compares with $N(E_F) = 5.4 \times 10^{34}$/erg-cm^3 and $I = 9.65 \times 10^{-14}$ erg reported by Féron and Pauthenet (14). These experimental values compare favorably with the theoretical $N(E_F) = 3.78 \times 10^{34}$/erg-cm^3 found by Keeton and Loucks (43) using the relativistic augmented plane wave method. The calculation for terbium gave $N(E_F) = 5.74 \times 10^{34}$/erg-cm^3 and $I = 4.3 \times 10^{-14}$ erg. This compares with $N(E_F) = 4.95 \times 10^{34}$/erg-cm^3 reported by Féron and Pauthenet (14). These experimental values also compare favorably with the theoretical value $N(E_F) = 3.30 \times 10^{34}$/erg-cm^3 determined by Jackson (44).

Work done on other rare earth metals confirms these figures. Cooper and Redington (45) have done infrared absorption work which showed that $N(E_F)$ changes only slightly over the range of the heavy rare earth metals. Lounasmaa (46) reported some measurements of electronic specific heat on Lutetium and dysprosium which gave a calculated $N(E_F) = 7 \times 10^{34}$/erg-cm^3. Watson *et al.* (47) showed that the interaction energy, I, was nearly constant over the range of the heavy rare earth metals Gd to Lu. The results obtained in this study agree with those above as well as might be expected for this method.

The "internal" fields calculated by equation (2.37) were 1.33×10^5 Oersteds for terbium and 4.0×10^5 Oersteds for gadolinium. This is a polarizing field localized outside the 4f shell as opposed to the commonly known internal field located at the ion site.

The critical field curve was used to give an estimate of the temperature at which holmium in zero applied field will square up into an anti-phase structure. As a sinusoidal structure begins to square up $\langle |m| \rangle_{\lambda} \rightarrow \sigma(0)$ and $\langle n \rangle_{\lambda} \rightarrow \bar{\sigma}$. So in the range from purely sinusoidal structure to anti-phase structure the right side of the equation (2.32) increases rapidly while the left side which is proportional to $\phi^2(T)$ (see Figure 19), is smoothly changing. Between 0 K and 15 K $\phi^2(T)$ changes very little, so any change in the critical field must be caused by continued transitions by ions into the anti-phase structure. The structure will be anti-phase then when H_c levels off. Figure 18 shows that this temperature was about 12 K.

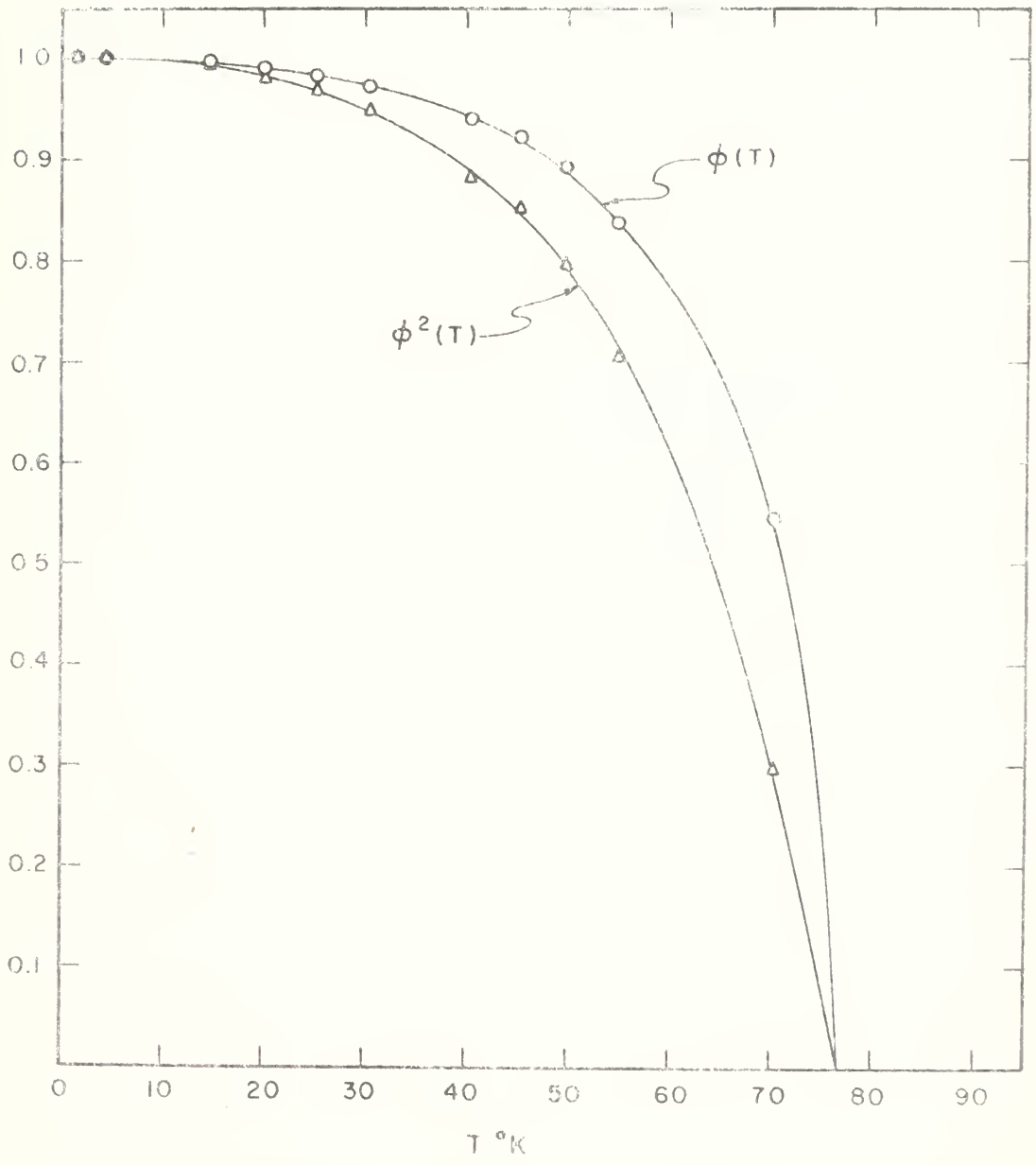

Figure 19. The reduced moment and the reduced moment squared as a function of temperature for holmium.

VI. LITERATURE CITED

1. Rudermann, M. A., and C. Kittel, Phys. Rev., 96, 99 (1954).

2. Nigh, H. E., S. Legvold, and F. H. Spedding, Phys. Rev., 132, 1092 (1963).

3. Hegland, D. E., S. Legvold and F. H. Spedding, Phys. Rev., 131, 158 (1963).

4. Jew, T. T. Magnetic anisotropy in dysprosium single crystals. Unpublished M.S. thesis. Ames, Iowa, Library, Iowa State University of Science and Technology (1963).

5. Strandburg, D. L., S. Legvold, and F. H. Spedding, Phys. Rev., 127, 2046 (1962).

6. Green, R. W., S. Legvold, and F. H. Spedding, Phys. Rev., 122, 827 (1961).

7. Richards, D. B. The high field magnetization of thulium single crystals. Unpublished Ph.D. thesis. Ames, Iowa, Library, Iowa State University of Science and Technology (1968).

8. Will, G., R. Nathaus, and H. A. Alperin, J. Appl. Phys., 35 (3) Pt2, 1045 (1964).

9. Koehler, W. C., J. Appl. Phys., 36 (3) Pt2, 1078 (1965).

10. Cable, J. W., and E. O. Wollan, Phys. Rev., 165 (2), 733 (1968).

11. Graham, C. D. Jr., J. Appl. Phys., 36 (3) Pt2, 1135 (1965).

12. Corner, W. D., W. C. Roe, and K. N. R. Taylor, Proc. Phys. Soc. (London) 80, 927 (1962).

13. Rhyne, J. J., S. Foner, E. J. McNiff, and R. Dodo, Jour. of Appl. Phys., 39, 892 (1968).

14. Féron, J. L., and R. Pauthenet Magnetocrystalline properties of rare-earth single crystals. Unpublished paper presented at Seventh Rare Earth Research Conference, Coronado, California, October 28, 1968. Laboratorie d'Electrostatique et de Physique du Métal, C.N.R.S. - B.P. 459, 38 - Grenoble, France. (1968).

15. Nellis, W. J. Thermal conductivity and Lorenz function of gadolinium, terbium, and holmium single crystals. Unpublished Ph.D. thesis. Ames, Iowa, Library, Iowa State University of Science and Technology (1968).

16. Sill, L. R., and S. Legvold, Phys. Rev., 137, A1139 (1965).

17. Lee, R. S., and S. Legvold, Phys. Rev., 162, 431 (1967).

18. Koehler, W. C., H. R. Child, E. O. Wollan, and J. W. Cable, J. Appl. Phys., 34, 1335 (1963).

19. Dietrich, O. W., and J. Als-Nielsen, Phys. Rev., 162 (2), 315 (1967).

20. Koehler, W. C., J. W. Cable, M. K. Wilkinson, and E. O. Wollan, Phys. Rev., 151 (2), 414 (1966).

21. Koehler, W. C., J. W. Cable, H. R. Child, M. K. Wilkinson, and E. O. Wollan, Phys. Rev., 158 (2), 450 (1967).

22. Dekker, A. J. Solid State Physics. Englewood Cliffs, New Jersey, Prentice-Hall, Inc. (1957).

23. Heisenberg, W., Zeitschrift für Physik, 49, 619 (1928).

24. Elliott, R. J., Phys. Rev., 124, 346 (1961).

25. Ziman, J. M. Principles of the Theory of Solids. London, England, Cambridge University Press (1964).

26. Ruderman, M., and C. Kittel, Phys. Rev., 96, 99 (1954).

27. de Gennes, P. G., Compt. Rend. Acad. Sci., 247, 1836 (1958).

28. Liu, S. H., Phys. Rev., 121, 451 (1961).

29. Liu, S. H., Phys. Rev., 123, 470 (1961).

30. Yosida, K., Phys. Rev., 106, 893 (1957).

31. Foner, S., Rev. Sci. Inst., 30, 548 (1959).

32. Powell, R. L., M. D. Bunch, and R. J. Corruccini, Cryogenics, 1, 139 (1961).

33. Rhyne, J. J. Magnetostriction of dsyprosium, erbium, and terbium single crystals. Unpublished Ph.D. thesis. Ames, Iowa, Library, Iowa State University of Science and Technology (1965).

34. Argyle, B. E., S. H. Charap, and E. W. Pugh, Phys. Rev., 132, 2051 (1963).

35. Danan, H. C., Compt. Rend. Acad. Sci., 246, 73 (1958).

36. Danan, H. C., A. Herr, and A. J. P. Meyer, J. Appl. Phys., 39 (2), 669 (1968).

37. Freeman, A. J., N. A. Blum, S. Foner, R. B. Frankel, and E. J. NcNiff Jr., J. Appl. Phys., 37, 1338 (1966).

38. Herring, C., R. M. Bozorth, A. E. Clark, and T. R. McGuire, J. Appl. Phys., 37, 1340 (1966).

39. Bozorth, R. M. Ferromagnetism. New York, N.Y., D. Van Nostrand Company, Inc. (1951).

40. Spedding, F. H., and J. E. Powell, J. Metals, 6, 1131 (1954).

41. Nigh, H. E., J. Appl. Phys., 34, 3323 (1963).

42. Edwards, L. R. Transport Properties of thulium single crystals. Unpublished Ph.D. thesis. Ames, Iowa, Library, Iowa State University of Science and Technology, (1967).

43. Keeton, S. C., and T. L. Loucks, Phys. Rev., 168, 672 (1968).

44. Jackson, C. The Electronic Structure of Terbium using the Relativistic Plane Wave Method. Phys. Rev. (to be published).

45. Cooper, B. R., and R. W. Redington, Phys. Rev. Ltrs., 14, 1066 (1965).

46. Lounasmaa, O. V., Phys. Rev., 126, 1352 (1962).

47. Watson, R. E., A. J. Freeman, and J. P. Dinmock, Phys. Rev., 167, 497 (1968).

VII. ACKNOWLEDGMENTS

The author would like to thank Dr. Sam Legvold for much advice rendered and especially for his encouragement during the frequent difficult days spent on this study.

Special thanks are due to Dr. D. B. Richards and Dr. L. R. Edwards for initial construction of the apparatus and subsequent advice and work on the apparatus.

Thanks are due to Dr. C. A. Swenson for several helpful discussions.

The author is also grateful to Dr. W. J. Nellis, Mr. J. L. Broderick, Mr. A. R. Harvey, Mr. D. W. Mellon, and Mr. C. Eagen for many interesting and sometimes productive discussions.

The author thanks the United States Navy for providing salary and five years to pursue this study.

Finally the author is most grateful to his wife, Jacquelyn, for the years of patience and encouragement and for typing the rough draft of this dissertation.

VIII. APPENDIX

A. Tabulation of Data

σ is in emu/g, H is in kOe

1. Single Foner data

Table 1. Magnetization of Gd c-axis at 4.2°K

run: I		II		III		IV		V	
σ	H_{int}	σ	H_{int}	σ	H_{int}	σ	H_{int}	σ	H_{int}
265.0	5.2	264.9	6.1	265.9	6.5	267.0	6.6	266.3	6.6
266.0	13.7	265.4	14.1	266.4	14.8	267.3	14.6	266.5	15.0
266.5	22.5	265.9	23.0	267.0	23.4	267.7	23.0	266.7	23.5
266.6	31.9	266.0	32.6	267.3	32.4	267.8	32.6	267.1	32.5
266.4	41.4	266.4	41.1	268.0	41.6	268.0	41.4	267.2	41.6
266.2	50.6	267.3	51.0	268.5	50.8	268.2	50.8	267.9	51.0
266.6	60.0	267.5	60.4	268.7	60.0	268.5	60.0	268.2	60.0
267.1	69.8	267.9	70.0	268.8	69.3	268.5	69.6	268.5	69.7
267.5	79.4	268.2	79.4	269.0	78.7	268.6	78.9	268.8	79.2

Table 2. Magnetization of Tb b-axis at 4.2°K

run: I		II		III	
σ	H_{int}	σ	H_{int}	σ	H_{int}
285.5	3.8	334.9	3.6	328.3	2.2
311.7	11.3	335.0	11.7	329.2	10.0

Table 2. (Continued)

run: I		II		III	
σ	H_{int}	σ	H_{int}	σ	H_{int}
316.3	20.3	335.3	20.4	329.6	19.4
318.6	29.6	335.5	29.8	330.6	29.6
320.3	39.1	335.9	38.7	331.4	39.0
320.3	48.7	336.3	48.1	332.2	48.8
321.2	57.7	336.7	57.3	333.1	58.8
322.1	67.2	338.5	66.5	333.8	68.3
		338.8	76.1	334.0	78.0

Table 3. Magnetization for H_o (b-axis) -- these isotherms were used to determine the critical field as a function of temperature

4.2°K		12.8°K		21.4°K		30.1°K		42.3°K		52.6°K		60.3°K		70.2°K	
σ	H_{int}	σ	H_{int}	σ	H_{int}	σ	H_{int}	σ	H_{int}	σ	H_{int}	σ	H_{int}	σ	H_{int}
16.1	0.3	45.3	0.7	25.6	0.8	17.3	3.5	9.4	2.6	70.3	13.4	81.4	14.9	91.3	18.2
42.8	0.6	111.9	0.7	60.2	3.2	28.1	5.3	34.8	7.5	128.0	14.3	112.0	16.6	111.1	19.5
95.8	0.7	165.3	1.0	131.9	3.2	74.4	6.9	80.0	10.8	200.2	14.9	187.5	17.0	152.0	20.1
148.8	0.8	211.4	1.7	204.1	3.7	154.3	7.1	159.1	11.3	231.4	17.9	219.3	20.0	203.8	20.2
200.3	1.1			278.8	4.4	231.9	7.6	236.8	11.9						
255.1	1.6														
295.4	3.2														
305.8	6.3														
309.6	9.9														

2. Double Foner data

All these data were taken at $4.2^{o}K$.

Table 4. Magnetization of Gd(c-axis), Tb(b-axis), Dy(a-axis), Ho(b-axis), and Tm(c-axis)

Gd		Tb		Dy		Ho		Tm	
σ	H_{int}	σ	H_{int}	σ	H_{int}	σ	H_{int}	σ	H_{int}
278.0	18.2	300.1	20.3	334.2	19.1	343.6	7.9	217.6	27.6
279.8	27.7	302.8	28.3	338.9	27.0	350.5	16.9	238.4	37.3
281.7	37.2	306.2	36.5	342.3	36.0	357.3	28.0	241.6	48.1
283.9	46.7	308.6	45.2	345.5	44.8	360.1	37.4	244.2	57.0
285.6	56.2	309.6	53.9	355.7	54.5	362.4	47.0	245.9	66.7
287.6	65.6	312.8	63.2	361.3	63.3	365.6	56.9	247.5	76.2
289.7	75.3	314.1	72.1	364.5	73.3	368.2	66.3		

B. Dimensions and Purity of Samples

Table 5. Dimensions of single Foner samples

	weight (gm.)	diameter (in.)
Fe I	.06801	0.100
Fe III	.11945	0.123
Gd	.07351	0.100
Tb	.08603	0.096
Ho	.07674	~0.090

Table 6. Dimensions of double Foner samples

	weight (gm.)	length (in.)	diameter (in.)
Tm	0.12921	0.0778	0.1200
Dy	0.08090	0.0684	0.1024
Tb	0.08964	0.0575	0.1221
Ho	0.08539	0.0512	0.1224
Gd	0.09630	0.0665	0.1227

The iron samples for use in the double Foner system had masses of 0.13046, 0.12693, 0.14322, 0.12593, 0.12350, and 0.12491 grams. They were all cylindrical disks of length about 0.080 inches.

The iron samples were cut from a section provided by Battelle Memorial Laboratory and Dr. C. W. Chen of the Metallurgy Department of this university. The resistivity ratio for the iron was given as $(\rho_{300}/\rho_{4.2}) = 230$.

Table 7. Purity of the samples used in this study --all figures are in ppm

	Fe	Gd	Tb	Dy	Ho	Tm
O_2	1.1	1506	719	209	421	458
N_2	<0.2					
H_2	0.09					
C	10	75				
S	0.5					
Al	-	<20	<60	40		<60
As	0.4					

Table 7. (Continued)

	Fe	Gd	Tb	Dy	Ho	Tm
B	<0.001					
Ca	2	<30	60	300	<300	<20
Cr	10	70	<100			<20
Co	10					
Nb	<0.05					
Cu	1.5	30	<20	-		-
Ge	<1.5					
Mg	3	<1	<20	70		<10
Hg	0.3					
Mo	0.8					
Ni	4	<100	<20			<50
P	1.2					
K	0.2					
Si	<2	<20	40	20	<<50	<60
Ag	0.04					
Na	0.012					
Ta	7	500	<1000	400	<500	
Sn	0.08					
Ti	0.6					
W	0.04					
V	0.3					
Zn	<0.7					
Zr	<0.1		<100			

Table 7. (Continued)

	Fe	Gd	Tb	Py	Ho	Tm
Fe		90	90	100	<50	<50
Eu		<<100				
Sm		<200	<300			
Y		<<100	<80	10	<50	<200
Tb		~200		1000		
F		25				
Dy			100		<50	-
Gd			<20	200		
Th]			<600			
Ho				100		<200
Er				50	<200	<30
Tm					<200	
Yb					<50	<10
Lu						<200

C. Discussion of Errors

Magnetization values were realized by using equation (3.1),

$$\sigma_x(Ha,\ T) = \frac{m_{Fe} G_x(Ha,\ T) F(T)}{m_x G_{Fe}(Ha,\ T') F(T')}\ \sigma_{Fe}(Ha,\ T').$$

The sample weights were in the region of 70 milligrams with a weighing error of $\pm$ .05 milligrams which gave a possible error of $\pm$ 0.07% in the sample weights. The factor F(T) was a correction of only 1% over the entire range

of temperature and reproduced to within 2%; thus it gave an error of about $\pm$ 0.02%. The error in σ_{Fe}(Ha, T) was good to $\pm$ 0.2% at high temperatures and to $\pm$ 0.1% at low temperatures with no applied field. The high field susceptibility of the iron could give an error of between 0.2% and 0.5% at 100 kilo-Oersteds depending on the value of high field susceptibility chosen.

The resolution of the apparatus was on the order of $\pm$ 0.00005 on the Gertsch ratio transformer. For the ferromagnetic samples run here, Gertsch readings ran typically in the region 0.40000 so the error was $\pm$ 0.01%. The accuracy of the Gertsch ratio transformer was (.001/ratio)%. Hence for large moments the error was $\pm$ 0.002%. The phase shift through the ratio transformer was $<$ 0.05 milliradian, which was negligible. The phase shifts in the circuit were estimated to cause an error of $\pm$ 0.01% because a change by a factor of ten in the capacitance in the quadrature circuit caused a change of only 0.00001 in the Gertsch ratio reading.

Centering was estimated to cause a $\pm$ 0.1% error. Vertical centering was conducted throughout a run. However, horizontal centering was done only at the beginning of a data run. Even when checking the horizontal centering following a run, the change in Gertsch ratio readings were rarely more than $\pm$ 0.0005 which is a $\pm$ 0.05% error.

The greatest source of error was the phenomenon of non-reproducible magnetic images. On a good day when several calibration isotherms of iron were run, the Gertsch ratio values would reproduce to within $\pm$ 0.1% from one isotherm to another. At other times the calibration curves would not reproduce to better than 1%. By selecting as the normalizing data that which was taken on days with good calibration reproducibility, it was thought that the accuracy of the spontaneous saturation magnetization was

accurate to within $\pm$ 0.2%. Because of the small size of the effect, the values for high field magnetic susceptibility are reliable to within $\pm$ 15%.